

Graphene-based spintronics

Cite as: Appl. Phys. Rev. 11, 021308 (2024); doi: 10.1063/5.0191362

Submitted: 13 December 2023 · Accepted: 12 March 2024 ·

Published Online: 15 April 2024



Gaojie Zhang,^{1,2} Hao Wu,^{1,2} Li Yang,^{1,2} Wen Jin,^{1,2} Wenfeng Zhang,^{1,2,3} and Haixin Chang^{1,2,3,a}

AFFILIATIONS

¹State Key Laboratory of Material Processing and Die & Mold Technology, School of Materials Science and Engineering, Huazhong University of Science and Technology, Wuhan 430074, China

²Wuhan National High Magnetic Field Center and Institute for Quantum Science and Engineering, Huazhong University of Science and Technology, Wuhan 430074, China

³Shenzhen R&D Center of Huazhong University of Science and Technology, Shenzhen 518000, China

Note: This paper is part of the APR Special Topic on New Carbon Materials.

^aAuthor to whom correspondence should be addressed: hxchang@hust.edu.cn

ABSTRACT

Graphene, the first isolated two-dimensional atomic crystal, is about to pass its 20th year. The last decade has been a critical period for graphene to gradually move from the laboratory to practical applications, and the research on the spin-related physical properties and various spintronic applications of graphene is still enduring. In this review, we systematically retrospect the important and state-of-art progresses about graphene-based spintronics. First, spin-orbit coupling and various tuning means in graphene have been introduced, such as adatoms, electrical control, and the proximity effect. Second, several methods for inducing magnetism in graphene are summarized, including defect, atom doping, proximity effect, and the recently attractive twisted magic-angle. Third, graphene-based lateral and vertical spin valves are discussed, along with some emergent spin transport properties, including spin injection, scattering, and relaxation. Fourth, graphene-based spin logic circuits for spin communications and multifunctional spin logic devices are exhibited. Finally, some significant opportunities and challenges of graphene-based spintronics for the fundamental physics and practical applications in the future are briefly discussed.

Published under an exclusive license by AIP Publishing. <https://doi.org/10.1063/5.0191362>

TABLE OF CONTENTS

I. INTRODUCTION.....	1
II. SPIN-ORBIT COUPLING IN GRAPHENE.....	2
III. MAGNETISM IN GRAPHENE.....	3
IV. GRAPHENE-BASED LATERAL SPIN VALVE AND SPIN TRANSPORT.....	7
V. GRAPHENE-BASED VERTICAL SPIN VALVE.....	10
VI. GRAPHENE-BASED SPIN LOGIC CIRCUITS	11
VII. CONCLUSION AND OUTLOOK.....	12

I. INTRODUCTION

Spintronics is an important research field in physics and materials science, aiming to utilize the spin freedom degree of electrons in materials to construct novel information storage and logic devices.¹ The concept arose from the discovery of the giant magnetoresistance effect in multilayers in 1988, followed by the discovery of the colossal magnetoresistance effect in perovskite manganese-based oxides in 1993 and the tunneling magnetoresistance effect in magnetic tunnel junctions in 1995.^{2–4} Subsequently, magneto-resistive materials related

to spin-polarized electron transport and new spintronic devices have also been developed.^{5–8} Since the successful isolation of graphene from graphitic carbon in 2004, the studies of graphene-based electronics and spintronics have attracted many attention from the scientific community due to the high mobility of $\sim 10\,000\text{ cm}^2/\text{V s}$ and long spin diffusion lengths of several micrometers at room temperature.^{9–15} Also, graphene exhibits many spin-related physical properties, such as gate-tunable spin-orbit coupling (SOC),^{16–18} proximity-induced ferromagnetism,^{19–28} moiré magnetism,^{29–34} spin Hall effect (SHE),^{35,36} quantum spin Hall effect (QSHE),³⁷ quantum anomalous Hall effect (QAHE),^{38–41} and unconventional superconductivity.⁴²

In the past decade, a series of advanced progresses in the field of graphene-based spintronics were emerged, such as SOC manipulation,^{16,39,40,43–49} magnetism introduction,^{26,38,50–53} unconventional magic-angle properties,^{29–34,42,47,54} the investigation of spin diffusion lengths,^{55,56} spin injection efficiency,^{57,58} and spin-filtering effect^{59,60} as well as the fabrication of spin logic operation with effective long spin communications.^{61–64} In this review, some important reports about graphene-based spintronics and the latest research progress in recent ten years are systematically reviewed. Section II introduces the

manipulation of SOC in graphene. Section III discusses the magnetic graphene and their magnetism origin. Sections IV and V reviews the graphene-based lateral and vertical spin valves as well as related spin transport properties, including spin injection, scattering, and relaxation. Section VI describes the graphene-based spin logic circuits. Section VII addresses potential opportunities and challenges for future prospects of graphene-based spintronics.

II. SPIN-ORBIT COUPLING IN GRAPHENE

SOC is a crucial spin interaction^{7,8} that identifies the relationship between the spin and orbital degrees of freedom of coupled electrons, which provided a promising avenue to control the electron's spin. SOC has led to many novel physical effects in graphene, such as the giant SHE,³⁵ quantum Hall effect (QHE),^{48,65,66} QSHE,³⁷ QAHE,^{39,40,67} band inversion and helical edge states,⁶⁸ weak localization,⁶⁹ and the Kondo effect.⁷⁰ Notably, regulating and controlling the SOC is the focus of research in graphene-based spintronics.

Since the energy of SOC is in real atoms proportional to the second power of the atomic number (it would be fourth power only in hydrogen-like ions),⁷¹ the light element carbon has a weak SOC (~ 7.86 meV for $2p$ orbitals of the carbon ions¹⁰). For pristine graphene, the spin-orbit splitting of the σ band at Γ point is identified as ~ 8.8 meV that may directly originate from the SOC of carbon.⁷² Meanwhile, at the K point, the spin-orbit splitting of the Dirac point is identified as $\sim 24\text{--}50$ μ eV.^{72\text{--}74} This splitting originates from the hybridization of the p_z orbitals, which form the Dirac cone, d orbitals, and higher carbon orbitals.⁷² In graphene, SOC is strongly associated with the band structures. As shown in Fig. 1, a Dirac cone is formed at the Fermi level of graphene without the SOC. When introducing SOC, a gap is opened at the Fermi level while preserving their spin degeneracy. With the increase in a transverse electric field, the spin degeneracy is lifted by the Rashba effect, forming novel topological band structures.⁷²

Most SOC strength of graphene is evaluated through weak localization and/or weak antilocalization. Study of SOC is crucial for graphene-based spintronics, which can be tuned by various means such as adatoms,^{43,46,75\text{--}80} electrical control,^{16\text{--}18,81,82} and proximity effect^{44,45,83\text{--}93} with the spin-orbit splitting from few to hundreds of millielectron volt (meV). Adatoms reported in previous reports include hydrogen,^{43,75,77} fluorine,^{46,76} gold,⁸⁰ and lead.⁷⁹ Among them, hydrogen influences the SOC of graphene by locally producing sp^3 bonding.⁹⁴ A recent study performed a decrease in SOC scattering length

with the increase in the hydrogen adatom density, indicating the enhancement of Bychkov-Rashba-type (BR) SOC in a single-side semi-hydrogenated graphene [Fig. 2(a)].⁴³ Such enhancement has also been revealed by SHE.⁷⁵ Moreover, the SOC of fluorine atoms is the main reason for the greatly induced local SOC in fluorinated graphene.⁴⁶ First-principles calculations have revealed that the increase in SOC in fluorinated graphene is ~ 1000 times and ~ 10 times larger than that of pristine graphene and hydrogenated graphene, respectively.⁴⁶ Figure 2(b) performed the spin-orbit splittings of single-side semi-fluorinated graphene for the three bands around the Fermi level. Furthermore, compared with the light adatoms, heavy adatoms induce more remarkable SOC by their own orbitals and result in a deep change of the local electronic structure of graphene.^{79,80} For example, Rader *et al.* reported a very large spin-orbit splitting of ~ 100 meV in Au-intercalated graphene/Ni interface and attributed it to hybridization with Au $5d$ states.⁸⁰ Also, theoretical tight-binding calculations show that 0.1% Pb adatoms can generate SOC of the order of ~ 40 meV that originates from the outer-shell p orbitals of Pb.⁷⁹

Till now, electrical modulation of graphene's SOC has been performed in graphene/Pb(Zr₅₂Ti₄₈)O₃,¹⁶ graphene/WS₂,^{17,18} and dilute fluorinated graphene.⁸² Park *et al.* reported a nonvolatile modulating SOC of graphene by ferroelectric dipole [Fig. 2(c)] and extracted the variations in SOC by using weak localization within the quantum interference theory.¹⁶ The advantage of ferroelectric gating modulation is that it changes the SOC strength of graphene without changing the charge neutral point. As shown in Fig. 2(d), with the increase in the poling voltage, the asymmetric and symmetric spin-orbit scattering rates are enhanced, which is ascribed to the spin-valley coupling of the effective electric field from the ferroelectric substrate.⁹⁵ Moreover, SOC can also be evaluated by Shubnikov-de Haas (SdH) oscillations, which has given an powerful evidence of the zero-field spin-splitting in bilayer graphene.¹⁷ First-principles calculations have exhibited that the SOC in fluorinated graphene can be effectively regulated by both the type and concentrations of carriers.⁸² Specifically, SOC will be increased or decreased by electron or hole doping, respectively, providing a potential possibility for electrical control of SOC in graphene. Moreover, electrical-field tunable SOC in graphene opens a novel avenue for the manipulation of spin-dependent transport properties and spin-orbitronic applications of graphene.

The proximity coupling effect through heterostructure engineering is an another way for SOC manipulation in graphene, which has

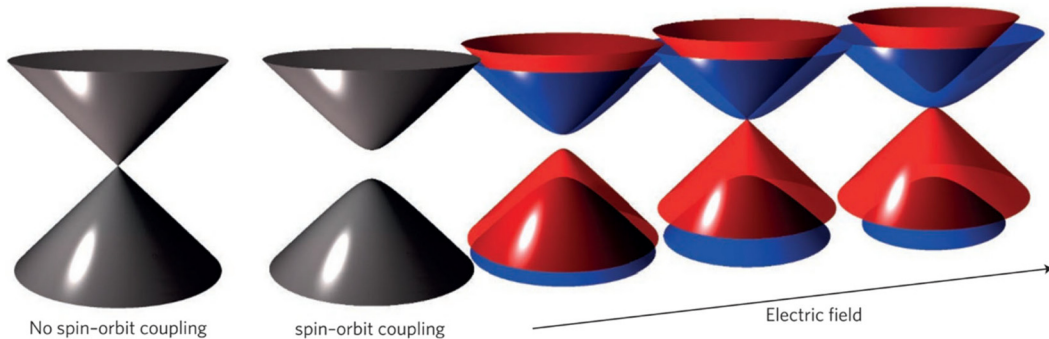


FIG. 1. Band structures evolution of graphene with or without SOC under a transverse electric field. Reproduced with permission from Han *et al.*, Nat. Nanotechnol. **9**, 794 (2014). Copyright 2014 Springer Nature.

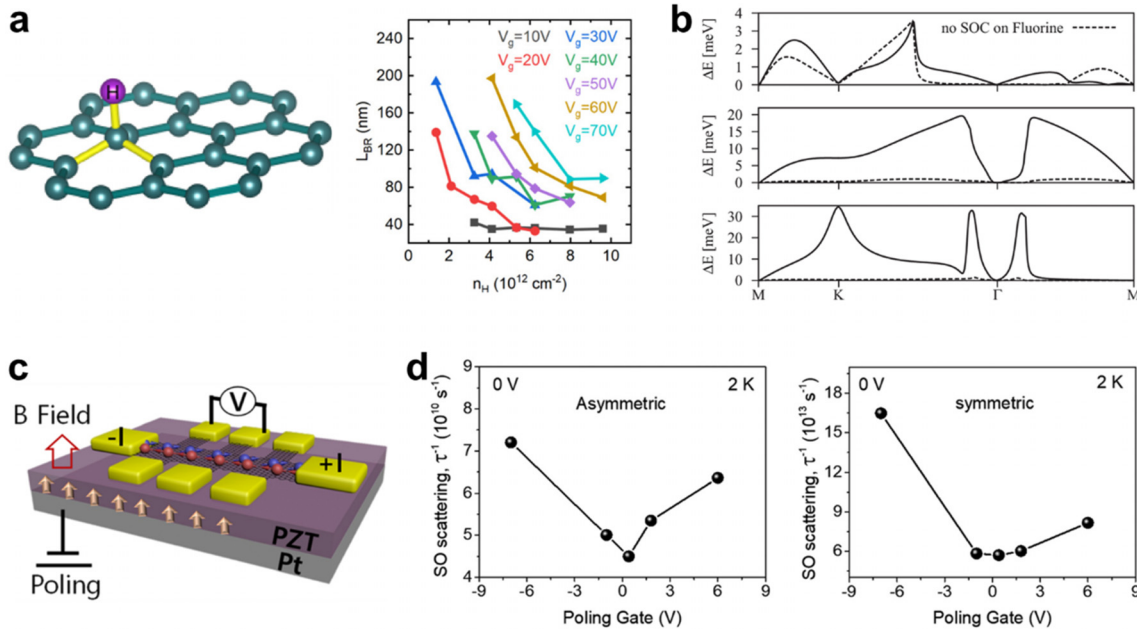


FIG. 2. Tuning SOC in graphene by atom doping and electric field. (a) Schematic of a hydrogenated graphene and corresponding hydrogen adatom density n_H dependence of the BR SOC scattering length L_{BR} . Reproduced with permission from Cao *et al.*, Phys. Rev. B **104**, 125422 (2021). Copyright 2021 American Physical Society. (b) Calculated band splittings of SOC in the single-side fluorinated graphene. Dashed lines show the band splittings of the fluorine adatom without SOC. Reproduced with permission from Irmer *et al.*, Phys. Rev. B **91**, 115141 (2015). Copyright 2015 American Physical Society. (c) Schematic of the structures of graphene-based Hall devices on the ferroelectric substrate, $\text{Pb}(\text{Zr}_{52},\text{Ti}_{48})\text{O}_3$. (d) Poling voltage dependence of the asymmetric and symmetric spin-orbit scattering rates at 2 K. Reproduced with permission from Park *et al.*, Appl. Phys. Lett. **117**, 203101 (2020). Copyright 2020 AIP Publishing.

been demonstrated in many coupled materials, such as WSe_2 ,^{44,45,48,68} WS_2 ,^{39,88,92} $\text{Pb}/\text{Ir}(111)$,⁸³ $\text{W}_x\text{Mo}_{1-x}\text{Se}_2$,⁹³ $\text{Bi}_{1.5}\text{Sb}_{0.5}\text{Te}_{1.7}\text{Se}_{1.3}$,⁸⁵ $\text{Pb}/\text{Pt}(111)$,⁸⁶ and some other transition metal dichalcogenides.^{87,89,90} As we all know, the strength of the proximity effect is strongly related to the interlayer coupling between the layers, which can be tuned by pressure,⁴⁴ stacking order,⁴⁵ and twist angle^{49,89,90} of the heterostructures. For instance, Fülöp *et al.* reported a graphene/ WSe_2 heterostructure device in which the distance between WSe_2 and graphene can be effectively regulated by changing a hydrostatic pressure, as shown in Fig. 3(a).⁴⁴ With the increase in pressure, the evolution from weak localization to weak antilocalization is emerged, indicating the increasing proximity-induced SOC in the graphene [Fig. 3(b)]. An obvious tendency of the decrease in the asymmetric scattering time τ_{asy} also suggests the increase in interlayer coupling, which further improves the SOC [Fig. 3(c)]. The raising scattering rates result to an enhancement of the Rashba parameter λ_R , clearly confirming the successful manipulation of the SOC strength [Fig. 3(d)]. Importantly, a pioneering experiment from Island *et al.* directly confirms the layer-selective SOC proximity effect and spin-orbit-driven band inversion in bilayer graphene/ WSe_2 , which opens the avenue for engineering strong topological insulators and correlation quantum phases in graphene.⁶⁸ Moreover, when h-BN is used as a capping layer, the interlayer coupling changes with the stacking sequence of heterostructures, which also affects the SOC strength in graphene [Figs. 3(e) and 3(f)].⁴⁵ Very recently, QHE and QAHE are both experimentally realized in graphene spin-orbit-proximitized by WSe_2 and WS_2 , respectively, which further highlights the great potential for manipulating novel topological electronic states and spins in graphene^{39,48} [Figs. 3(g) and 3(h)].

Overall, considering the weak intrinsic SOC of pristine graphene, manipulating SOC in graphene provides more opportunities for graphene-based spintronic applications. Meanwhile, these manipulating techniques also have the potential to extend to other topological quantum materials, such as topological insulators, Weyl semimetals, superconductors, and 2D magnets.⁹⁶⁻⁹⁸

III. MANGETISM IN GRAPHENE

Pristine and perfect graphene only shows Landau orbital diamagnetism. Making graphene magnetic is conducive to further improving its multi-functionality. It is expected to further optimize computing speed, storage capacity, and power dissipation by effectively controlling and manipulating spin polarization, which is fundamentally important for the development of spintronics and the future electronics industry.^{10,99-101} The first step is to induce magnetic moment in graphene, and then, long-range magnetic order and technically controllable magnetism are necessary for suiting the demand of various spintronic devices. To date, there are many studies in theory and experiments for inducing magnetism in graphene by defects and edge states,^{51,102-107} light atom doping (e.g., H, F),^{50,104,105} heavy atom doping (e.g., 3d and 5d atoms),^{52,53,108} molecular doping,¹⁰⁹ ferromagnetic proximity,¹⁹⁻²⁷ and twisted magic-angle.^{29-34,110} Therefore, the origin of magnetism in graphene is also diverse.

For the magnetism induced by vacancy defects and atom doping, theoretical studies suggest that removing a single p_z orbital will give graphene a single π state at the Fermi level. However, the electrostatic coulomb repulsion forbade the occupation of two electrons with the same spin in this p state, resulting in only one occupation and further

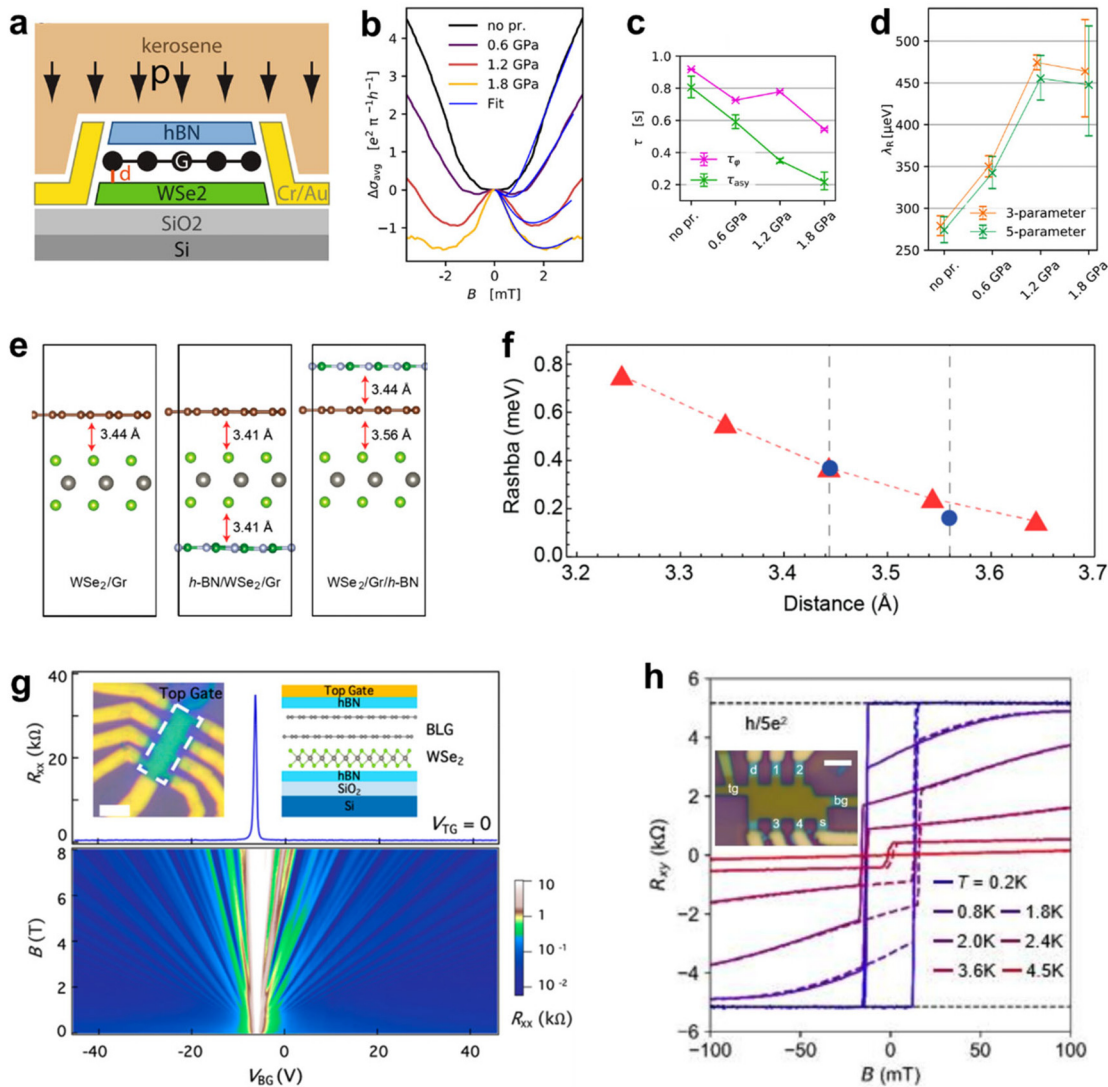


FIG. 3. Tuning SOC and magneto-transport in graphene by the proximity effect. (a) Schematic of an hBN/graphene/WSe₂ heterostructure in a pressure regulation device. (b) Magnetic field dependent averaged magneto-conductivity $\Delta\sigma_{\text{avg}}$ under different pressure at 4 V. (c) Pressure-dependent phase-breaking time τ_ϕ and asymmetric scattering time τ_{asy} due to SOC terms at 4 V. (d) Rashba parameter λ_R under different pressures. Reproduced with permission from Fülop et al., npj 2D Mater. Appl. **5**, 82 (2021). Copyright 2021 Springer Nature. (e) Calculated interlayer distances of WSe₂/graphene, h-BN/WSe₂/graphene, and WSe₂/graphene/hBN. (f) Interlayer distance dependent Rashba SOC strength of WSe₂/graphene (red circles). The blue circles are the Rashba SOC strength extracted from WSe₂/graphene and WSe₂/graphene/hBN in (e). Reproduced with permission from Yang et al., Nano Lett. **18**, 3580 (2018). Copyright 2018 American Chemical Society. (g) Back-gate voltage and magnetic field dependent R_{xy} at 1.5 K in graphene/WSe₂. Reproduced with permission from Wang et al., Nano Lett. **19**, 7028 (2019). Copyright 2019 American Chemical Society. (h) Magnetic field dependent R_{xy} in graphene/WSe₂ under different temperatures. Reproduced with permission from Han et al., arXiv:2310.17483 (2023). Copyright 2023 Arxiv.

produce a net magnetic moment.⁵⁰ It is predicted that one H atom chemisorption defect and one vacancy defect will produce magnetic moment of ~ 1 and $\sim 1.12\text{--}1.53 \mu\text{B}$, respectively. Whether the coupling is ferromagnetic or antiferromagnetic depends on defect in hexagonal sublattices,¹⁰⁴ and the origin of vacancy magnetism is regarded as itinerant magnetism or dangling bonds.¹⁰⁹ Moreover, transition metal atom doping will also cause local magnetic moments in graphene by enhanced conduction-electron mediated long-range magnetic interaction through hybridization between the d electrons of transition metal atoms and

delocalized p_z electrons of C atoms.⁵² For the edge states, it is predicted that crystallographic directions (e.g., armchair and zigzag) and the crystal edges can influence the magnetism in graphene. For example, it is regarded as the armchair graphene does not have magnetic moments, while the zigzag one shows the magnetic order due to the high density of low-energy states (or called flat energy dispersion bands), which may facilitate to the formation of magnetic spin polarization at edges.¹¹¹

Based on these, experimental realization of edge states and controllable generation of vacancies or adatoms in graphene lattice have

been achieved.^{50,51,102,103,105,114–116} Earlier studies used irradiation with high-energy particles (e.g., protons) to create carbon vacancies in graphite/graphene, thereby inducing magnetic moments.^{115,116} In 2016, González-Herrero *et al.*⁵⁰ directly realized atomic-scale control of magnetic moment with a ~ 20 meV spin splitting at the Fermi level in H-doped graphene by scanning tunneling microscopy (STM) [Fig. 4(a)]. Such H-doped graphene shows atomically tunable spin texture with few nanometers scale away from the H atom, thereby implying long-range magnetic interaction between magnetic moments [Fig. 4(b)]. Recently, the single-carbon vacancy induced tunable magnetism with three different magnetic moments (1.6, 0.5, and 0 μB) in graphene was also detected by spin-polarized STM tests.¹⁰³ Moreover, the edge ferromagnetism up to room temperature is realized in zigzag-edged graphene via epitaxy on h-BN templates, which is attributed to the superexchange interaction between local “unpaired” electrons located in the zigzag C-BN interface.¹⁰² Such edge ferromagnetism is directly confirmed by magnetic force microscopy (MFM) and magnetization tests, showing magnetic moment of $\sim 1 \times 10^{-4}$ emu/g at room temperature [Fig. 4(c)]. Hu *et al.*⁵² achieved robust above-room-temperature ferromagnetism

up to 400 K in Co-N₄ moiety doped graphene with sizeable magnetization of ~ 0.11 emu/g at room temperature [Fig. 4(d)]. Although many experimental results have been achieved, the magnetism induced by vacancy, edge states, and dopant usually very small and magneto-transport measurements is lacking, which is hard to use for potential spintronic applications.

In contrast, proximity-induced ferromagnetism characterized by magneto-transport tests (e.g., the anomalous Hall effect) directly proved the long-range ferromagnetic order and its electrical controllability in graphene-based heterostructures.^{19,21,23–27} Compared with defect/dopant-induced magnetism, the proximity-induced ferromagnetism has less effect on the electronic structure of graphene.²⁴ The use of electrically insulated ferromagnetic substrates is a prerequisite for confirming that this ferromagnetism originates from graphene. The enhanced exchange field and SOC introduced in graphene by the ferromagnetic substrate are the source of such proximate ferromagnetism, which is closely related to the strength of interfacial coupling.^{19,20,27} Recently, Song *et al.*²⁷ observed the anomalous Hall effect up to 80 K in graphene/Fe_xSn_{1-x}S₂ van der Waals heterostructures [Fig. 4(e)],

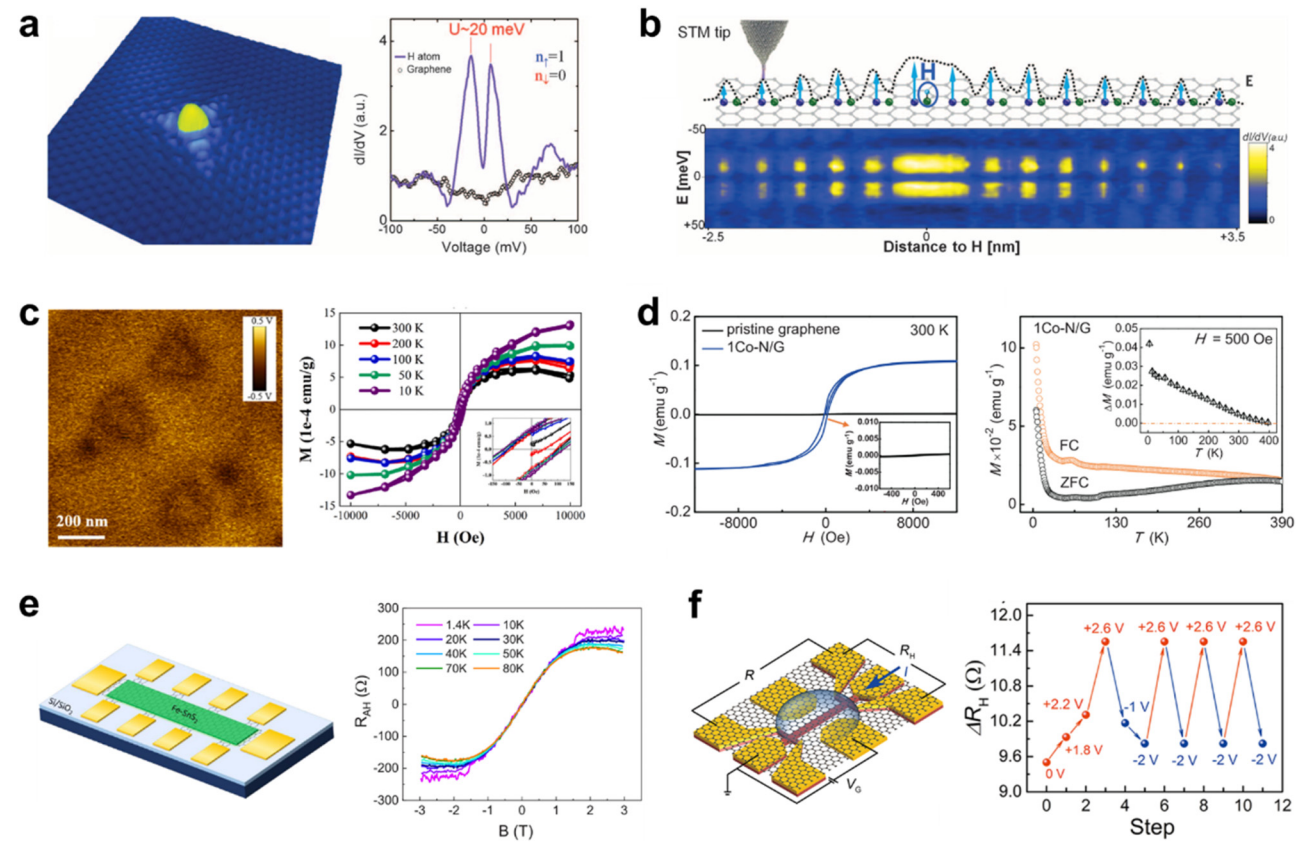


FIG. 4. Making magnetism in graphene by different approaches. (a) STM topography and spin splitting of an H atom in H-doped graphene. (b) Conductance map [$dI/dV(x, E)$] along an H atom direction. Reproduced with permission from González-Herrero *et al.*, Science **352**, 437 (2016). Copyright 2016 AAAS. (c) Edge magnetism in zigzag-edged graphene nanosheets embedded on h-BN proved by MFM and magnetization tests. Reproduced with permission from Ge *et al.*, Carbon **203**, 59 (2023). Copyright 2023 Elsevier. (d) Magnetization tests of pristine and Co-N₄ moiety doped graphene. Reproduced with permission from He *et al.*, Nat. Commun. **12**, 1854 (2021). Copyright 2021 Springer Nature. (e) Anomalous Hall effect induced by proximity coupling in graphene/Fe_xSn_{1-x}S₂ heterostructure. Reproduced with permission from Song *et al.*, Phys. Rev. B **103**, 125304 (2021). Copyright 2021 American Physical Society. (f) Electrical control of proximity ferromagnetism in Fe₃O₄/graphene heterostructure. Reproduced with permission from Liu *et al.*, Nano Lett. **22**, 4392 (2022). Copyright 2022 American Chemical Society.

companying with the enhancement of SOC. In addition, room-temperature ferromagnetism also can be realized in graphene enabled by ferromagnetic insulating substrates with above-room-temperature Curie temperature, such as Fe_3O_4 ($\sim 858 \text{ K}$)^{21,26} and yttrium iron garnet (YIG) ($\sim 550 \text{ K}$).¹⁹ Among them, the anomalous Hall resistance of Fe_3O_4 /graphene can be repeatedly and reversibly controlled through ionic liquid gating based on the pure protons migration [Fig. 4(f)].²⁶

Very recently, the discovery of a new van der Waals above-room-temperature intrinsic ferromagnetic semiconductor $\text{FeCr}_{0.5}\text{Ga}_{1.5}\text{Se}_{4.0}$ crystal with bandgap of $\sim 1.2 \text{ eV}$ further promotes the development of proximity-induced ferromagnetism in graphene.²⁸ As for a single 4.8 nm graphene-based Hall device, the straight lines with clear negative slope in Hall resistance curves under different temperatures demonstrate the electron-conduction type of graphene and non-ferromagnetic nature [Figs. 5(a) and 5(c)]. In contrast, as for a graphene/ $\text{FeCr}_{0.5}\text{Ga}_{1.5}\text{Se}_{4.0}$ (3.6/28 nm) heterostructure, a series of obvious inverted "S"-shaped anomalous Hall resistance curves appear ranging from 2 to 400 K [Figs. 5(d) and 5(f)]. This result confirms the conduction type transition (from electron to hole) and above-room-temperature intrinsic ferromagnetism in graphene. Notably, the anomalous Hall effect maintained at 400 K is attributed to the strong proximity coupling between $\text{FeCr}_{0.5}\text{Ga}_{1.5}\text{Se}_{4.0}$ and graphene, thereby implying the $\text{FeCr}_{0.5}\text{Ga}_{1.5}\text{Se}_{4.0}$ as an ideal substrate for proximity-induced ferromagnetism in graphene.

Furthermore, magic-angle graphene with the moiré flatband induced strong electron correlation also presents the intrinsic

ferromagnetism by delicately controlling the filling level of the flatband, which is fundamentally important for the development of the moiré physics and spintronics.^{29–34,110} For example, the near three-quarters filling of the conduction miniband promotes the twisted bilayer graphene (TBG) into the ferromagnetic state accompanied by the giant anomalous Hall resistance up to $\sim 10.4 \text{ k}\Omega$, which is attributed to the enhancement of electron-electron interactions caused by flat superlattice minibands [Fig. 6(a)].²⁹ The multiple intermediate steps around the coercive field likely originate from a mixture domain structure with different coercivity or a repetitive pattern of domain wall motion and pinning. Moreover, the residual anomalous Hall resistance only stabilizes in a very narrow of density (n/n_s) near 3/4 filling of the mini-Brillouin zone [Fig. 6(b)]. With the increase in temperature, the coercivity rapidly decreases and down to zero at 3.9 K, while the anomalous Hall resistance remains almost unchanged below 2.8 K and disappears at 5 K [Figs. 6(c) and 6(d)]. Meanwhile, the transport properties of magic-angle graphene can also be influenced by SOC. A transition from Mott-like insulators to ferromagnetic states at both half and quarters filling has performed in TBG/WSe₂ heterostructure interface with the obvious anomalous Hall effect [Figs. 6(e) and 6(f)].³⁰ However, no QAHE is observed in these systems. Breakthrough comes from the TBG aligned to h-BN, which shows QAHE when the temperature is below $\sim 5 \text{ K}$.³⁴ The quantum transport phenomenon is induced by intrinsic strong interactions, which polarize the electrons into a single spin- and valley-resolved moiré miniband with Chern number $C = 1$. Moreover, Berry-curvature-induced nanoscale equilibrium orbital magnetism is also directly imaged by continuously tuning

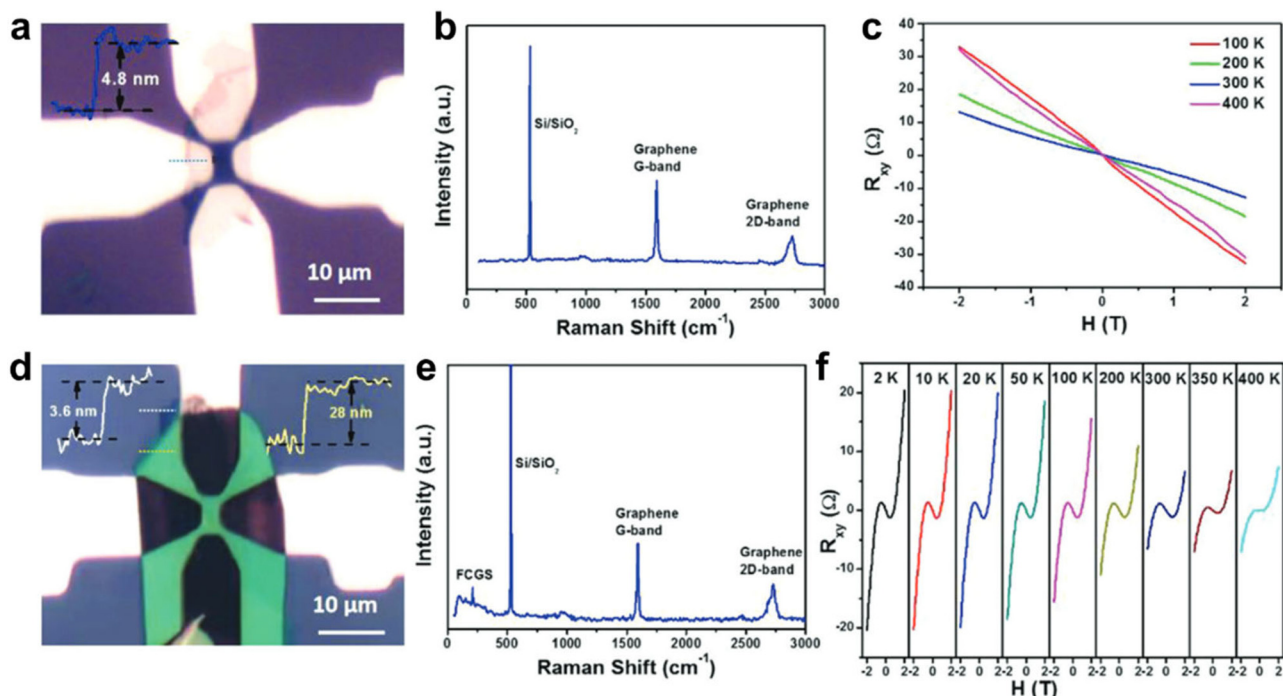


FIG. 5. Proximity-induced above-room-temperature ferromagnetism in graphene by using a new van der Waals above-room-temperature ferromagnetic semiconductor $\text{FeCr}_{0.5}\text{Ga}_{1.5}\text{Se}_{4.0}$. (a) and (b) Optical image and Raman spectra of an ultra-thin graphene-based Hall device. (c) Corresponding Hall resistance curves under different temperatures. (d) and (e) Optical image and Raman spectra of a graphene/ $\text{FeCr}_{0.5}\text{Ga}_{1.5}\text{Se}_{4.0}$ (3.6/28 nm) heterostructure. (f) Corresponding anomalous Hall effect under different temperatures. Reproduced with permission from Wu *et al.*, Small Methods 2301524 (published online) (2024). Copyright 2024 Wiley-VCH.

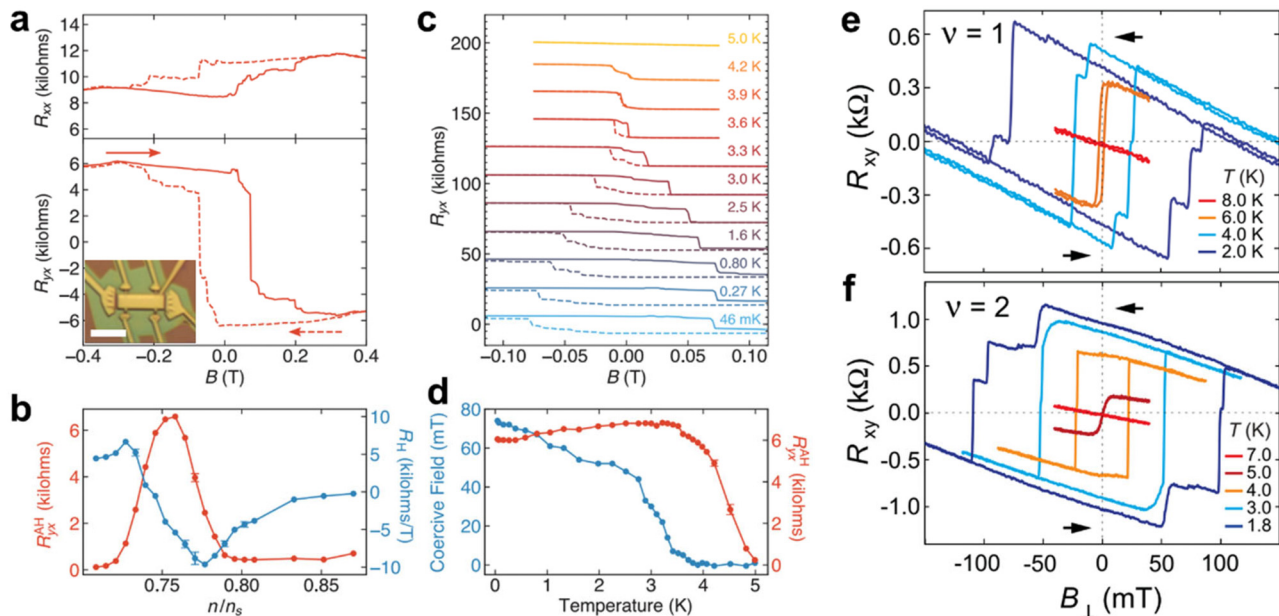


FIG. 6. Emergent ferromagnetism in magic-angle graphene. (a) Magnetic field dependent longitudinal resistance R_{xx} and Hall resistance R_{yx} of a twisted bilayer graphene. (b) n/n_s dependent zero-field anomalous Hall resistance R_{yx}^{AH} and ordinary Hall slope R_H . n is the carrier density, and n_s is the carrier density of charge neutrality point. (c) Magnetic field dependent R_{yx} under different temperatures. (d) Temperature-dependent coercivity and R_{yx}^{AH} . Reproduced with permission from Sharpe *et al.*, Science 365, 605 (2019). Copyright 2019 AAAS. Magnetic field dependent Hall resistance R_{xy} at $n = 0.55 \times 10^{12} \text{ cm}^{-2}$ near moiré filling $v = 1$ (e) and $n = 1.22 \times 10^{12} \text{ cm}^{-2}$ near moiré filling $v = 2$ (f) in the twisted bilayer graphene/WSe₂ interface. Reproduced with permission from Lin *et al.*, Science 375, 437 (2022). Copyright 2022 AAAS.

the filling factor.³³ In addition to emergent ferromagnetism, these amazing graphene-based moiré-patterned superlattices provide an important platform for tuning other novel physical properties, such as correlated insulating phase^{117,118} and unconventional superconductivity.⁴²

Despite these breakthroughs, any of the above methods for making graphene magnetic have limitations. Controlled creation of vacancy or atomic doping is challenging and magnetically weak, and the proximity effect is strongly related to the properties of the substrate and the coupling interaction of the interface. Moreover, many efforts are still needed to elucidate the underlying mechanisms of ferromagnetism in magic-angle graphene and explore novel spintronic applications based on these attractive properties. The ideal situation is to directly dilute the magnetic atom doping or other reliable methods to induce electrically detectable long-range magnetic order in free-standing graphene and then directly used them in-state-of-art spintronic devices.

IV. GRAPHENE-BASED LATERAL SPIN VALVE AND SPIN TRANSPORT

Generally, spin transport measurements are divided into two different types: “non-local” (NL) and “local” measurements, as shown in Fig. 7. Among them, the E_2 and E_3 are spin injecting and detecting electrodes, respectively. The spin-valve signal is identified as $\Delta R_{NL} = (V_{NL}^P - V_{NL}^{AP})/I_{inj}$, where the V_{NL}^P and V_{NL}^{AP} are measured voltages when the magnetization between ferromagnetic electrodes is parallel or antiparallel, respectively, and the I_{inj} is the injection current.¹⁰ Notably, the change of resistance in local and non-local measurements both originates from the spin accumulation, while the

latter has a higher signal-to-noise as there is no net charge flow between injecting and detecting electrodes. The first experiment for spin transport on graphene-based lateral spin valve was proposed as early as 2006 with ~10% change in resistance.¹¹⁹ Subsequently, a series of creative related studies on graphene were mostly carried out by different research groups between 2007 and 2013.^{12–14,120–122} However, most of these early works show relatively short spin lifetimes of a few hundred picoseconds and spin diffusion lengths below few micrometer, which are well below theoretical expectations.¹²³

Since 2014, some new and interesting works on graphene-based lateral spin valves have been implemented.^{36,55,124–128} Tables I and II summarize some spin transport properties, such as spin diffusion length (λ_s), spin-valve signal (ΔR_{NL}), spin lifetime (τ_s), and spin injection efficiency of these devices. For example, with the discovery of van

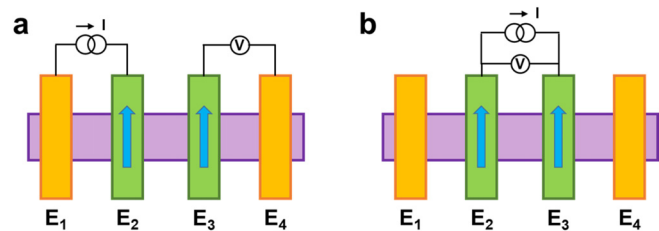


FIG. 7. Two different types of lateral spin valve measurement geometry. Non-local (a) and local (b) spin transport measurements. The purple strips are graphene, the green strips are ferromagnetic electrodes, the yellow strips are non-magnetic or ferromagnetic electrodes, and the blue arrows are magnetization directions.

TABLE I. Spin diffusion length (λ_s), spin-valve signal ($|\Delta R_{NL}|$), and spin lifetime (τ_s) of graphene-based lateral spin valves in the last decade.

Remarks	λ_s (μm)	$ \Delta R_{NL} $ ($\text{m}\Omega$)	τ_s (ps)	T (K)	Year	Ref.
NL, Fe_5GeTe_2	2.74	27.7	228	300	2023	127
NL, Co	1.2	47	...	50	2016	136
0.8–1	40	40–50	300	2017	125	
13	...	2500	300	2015	137	
2–3	368.7	...	300	2020	135	
3–6	20–4000	400–1200	300	2015	138	
3.04	4521.7	308	10	2017	139	
9	213	3000	300	2019	140	
0.85	20 000	...	8	2014	141	
30.5	1343.4	12 600	300	2016	56	
10	1000	250	77	2019	142	
13.6	1600	3500	300	2020	55	
NL, NiFe	0.15–0.98	6.9	2.02–66.05	30	2021	134
	1.5	3000	200	200	2014	143
Local, Co	5.8	800 000	900	300	2017	57
	6.5	16 200	740	75	2018	58

der Waals 2D ferromagnetic crystals,^{129–133} some graphene-based lateral spin valves with high-quality van der Waals ferromagnetic contact have also been realized in 2023^{124,127,128} [Fig. 8(a)]. However, these so-called “high-quality” interfaces do not exhibit obviously enhanced spin

TABLE II. Spin injection efficiency in graphene-based lateral spin valves with different tunnel barriers in the last decade.

Electrodes	Tunnel barriers	Spin injection efficiency (%)	Year	Ref.
Fe_3GaTe_2	No barrier	6	2023	128
Fe_3GeTe_2	No barrier	1	2023	124
Fe_5GeTe_2	No barrier	9.5	2023	127
Co	hBN	50	2017	57
	hBN	50	2018	58
	YO_x	15	2014	141
	TiO_x	12	2019	140
	TiO_x	12.5	2020	55
NiFe	AlO_x	8.4	2021	134
	Fluorinated-graphene	63	2014	143

transport properties so far (e.g., Fe_5GeTe_2 /graphene interface with spin diffusion length and spin injection efficiency only $\sim 2.74 \mu\text{m}$ and 9.5%, respectively¹²⁷), which should be further discussed and optimized. Actually, at room temperature, an extremely long spin communication performance ($\sim 45 \mu\text{m}$) with long spin diffusion length was reported in polycrystalline graphene with conventional Co ferromagnetic electrodes by Panda *et al.* in 2020 [Fig. 8(b)].⁵⁵ The exponential relation between ΔR_{NL} and channel length is ascribed to the different spin

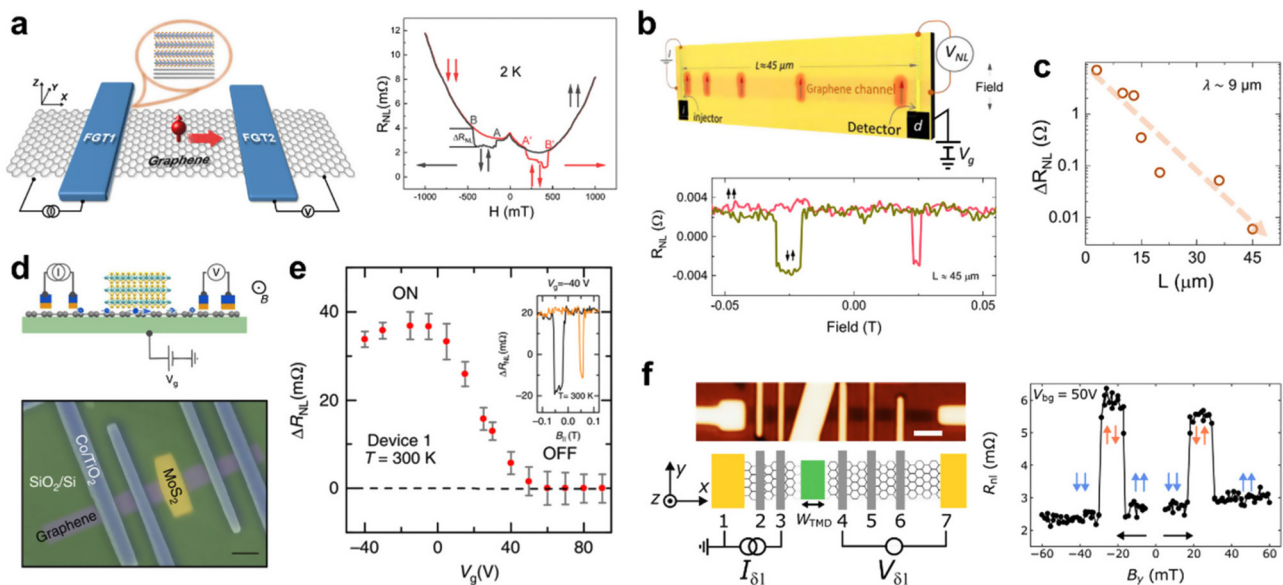


FIG. 8. Spin transport measurements in graphene-based lateral spin valves. (a) Non-local measurement at 2 K in a graphene/ Fe_3GeTe_2 van der Waals heterostructure. Reproduced with permission from He *et al.*, ACS Appl. Mater. Interfaces **15**, 9649 (2023). Copyright 2023 American Chemical Society. (b) Non-local measurement with a channel length $L \approx 45 \mu\text{m}$ at room temperature in graphene devices with Co/TiO_x electrodes. (c) Channel length L dependence of the ΔR_{NL} following the relation of $\Delta R_{NL} \approx e^{-L/\lambda}$. Reproduced with permission from Panda *et al.*, ACS Nano **14**, 12771 (2020). Copyright 2020 American Chemical Society. (d) Schematic and scanning electron microscopy (SEM) image of a graphene device with MoS_2 top gate and Co/TiO_x electrodes. (e) Gate voltage V_g dependent spin-valve signal ΔR_{NL} at 300 K. Inset shows a typical spin-valve magnetoresistance curve under gate voltage of -40 V at 300 K. Reproduced with permission from Dankert and Dash, Nat. Commun. **8**, 16093 (2017). Copyright 2017 Springer Nature. (f) Non-local spin transport measurement under back-gate voltage of 50 V at 50 K in a graphene-based lateral spin valves with the WSe_2 back gate. Reproduced with permission from Ingla-Aynes *et al.*, Phys. Rev. Lett. **127**, 047202 (2021). Copyright 2021 American Physical Society.

polarizations due to different doping and interface resistance in different devices [Fig. 8(c)]. In addition, spin transport on graphene can also be regulated through electrostatic gating of 2D semiconductors, such as MoS₂,¹²⁵ WSe₂,¹²⁶ [Figs. 8(d) and 8(f)], WS₂,¹³⁴ and TaS₂¹³⁵ at room temperature. For instance, with the increase in gate voltage, the ΔR_{NL} of the MoS₂-gated spin valve is basically unchanged in the -40 to 0 V (ON state), then gradually decreases in the 0 to 50 V, and finally down to zero in the over 50 V (OFF state) [Fig. 8(e)]. The effectively modulation of ON/OFF states depending on the ΔR_{NL} value by gate voltage at room temperature is fundamentally important for electrical control of spintronics.

Spin injection efficiency of the graphene/ferromagnet interface determines the spin accumulation that is technically important for enhancing spin output signals. However, conductivity mismatch between the ferromagnetic electrode and graphene results to the low spin injection efficiency, which originates from their different spin resistances.¹⁴⁴ Therefore, when the spin current is injected into graphene, a portion of the spin flow will backflow (spin flip) into the ferromagnetic electrode. Utilizing a tunnel barrier at interface will reduce this backflow behavior, thus improve the spin injection efficiency.^{13,57,58,141,143,145–147} It is worth mentioning that the ideal tunnel barrier is free of surface roughness and pinholes because the former will generate the non-uniform interfacial magnetization, and the latter will lead to the direct contact between graphene and the ferromagnetic electrodes.¹⁴⁸ All these factors improve the spin backflow, thereby leading to the reduction of spin injection efficiency. Since the bonding-free atomically flat nature of 2D van der Waals materials overcomes the lattice mismatch and surface roughness, the use of hBN^{57,58,145–147} and fluorinated-graphene¹⁴³ as the tunnel barriers shows high spin injection efficiency. Moreover, applying the bias voltage can further improve the spin injection efficiency in graphene-based spin valves.^{57,58,61} For example, hBN-based spin injection induced by bias

voltage shows an extremely high spin injection efficiency of 100% and a large spin signal of 800 Ω .⁵⁷

Furthermore, a main problem in graphene-based spintronics is a large difference of graphene's spin lifetime in theory and experiment. In general, the theoretical spin lifetimes of pristine graphene are $\sim 1 \mu\text{s}$ ($\sim 10^6 \text{ ps}$), whereas experimental values only range from tens of picoseconds to tens of nanoseconds ($\sim 10^1$ – 10^4 ps).^{55–58,125,127,134,137–140,142,143} At best, there is also a gap of about two orders of magnitude between them. This is because that the spin transport is affected by many external factors, namely, spin scattering, which will also affect the output spin signal. Scattering sources of graphene-based lateral spin valves are diverse, such as SOC originating from surface corrugation,^{61,149–152} grain boundaries,^{153,154} defect-induced charge traps,¹⁵⁵ contact-induced spin relaxation,^{55,56} and charge inhomogeneities.^{156,157} Moreover, an important theory that matches well with the experiments suggests that resonance scattering of local magnetic moments leads to observed short spin-relaxation times in graphene.¹⁵⁸ Some studies propose that the introduction of a high-quality hBN substrate can reduce the spin scattering in graphene.^{121,159,160} Nevertheless, the proper consensus on spin scattering mechanisms in graphene still should be further discussed.

A typical experimental method for evaluating the spin relaxation and spin precession in graphene is the Hanle spin measurement with non-local geometry [Fig. 9(a)]. This is done by applying a perpendicular magnetic field, which causes spin precession as the spin in graphene diffuses from the injection electrode to the detection electrode.¹⁰ Figure 9(b) presents a representative Hanle spin-precession curve and corresponding bias-dependent spin diffusion length and spin lifetime at 300 K.¹²⁵ Moreover, different spin polarization directions at the ferromagnet/graphene interface can also be probed by applying magnetic field along different directions, which has been done in Fe₅GeTe₂/graphene heterostructures.¹²⁷ Figures 9(c) and 9(e) show the schematic

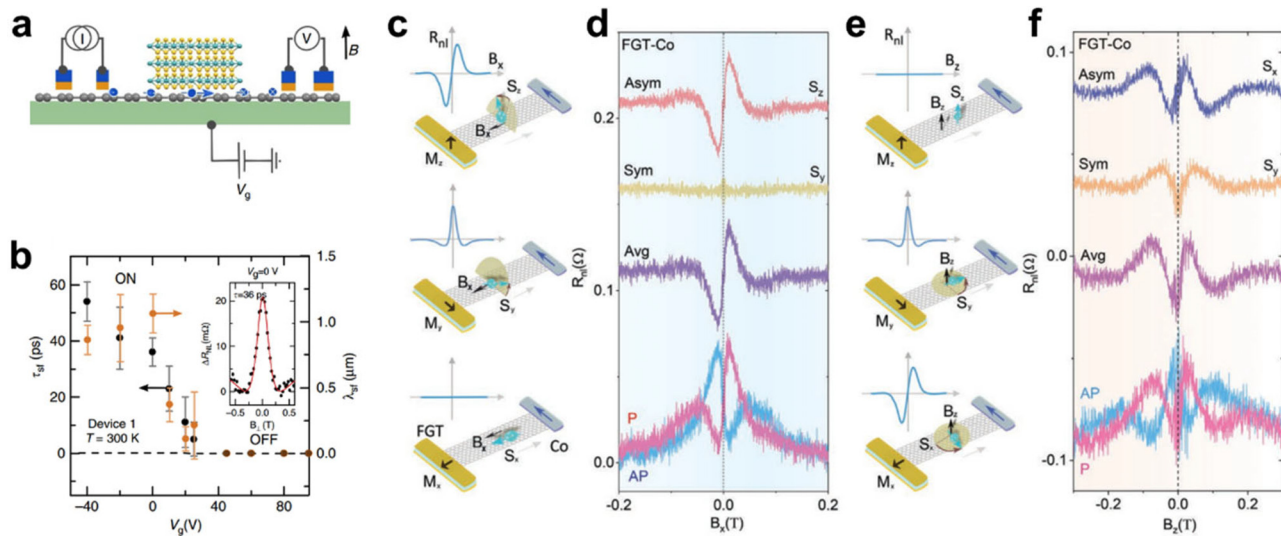


FIG. 9. Hanle spin relaxation and precession measurements based on graphene. (a) Schematic of gate-tunable non-local Hanle measurement based on graphene/MoS₂ with Co/TiO_x ferromagnetic electrodes. (b) Gate voltage dependence of spin lifetime τ_{sf} (black) and diffusion length λ_{sf} (orange). Inset is the Hanle spin signal measured without gate voltage. Reproduced with permission from Dankert and Dash, Nat. Commun. **8**, 16093 (2017). Copyright 2017 Springer Nature. (c)–(f) Schematics and measured Hanle spin signals of Hanle measurements under B_x and B_z field sweeps based on Fe₅GeTe₂/graphene heterostructures at room temperature. Reproduced with permission from Zhao et al., Adv. Mater. **35**, 2209113 (2023). Copyright 2023 Wiley-VCH.

of xHanle and zHanle tests for three spin components (S_x , S_y , and S_z) injected from Fe_5GeTe_2 with three magnetizations (M_x , M_y , and M_z). It is worth noting that the spin will not precess when the magnetic field and the spin direction are collinear, thereby leading to the absence of Hanle signal. The sine-shaped xHanle signal is attributed to the perpendicular magnetic anisotropy of Fe_5GeTe_2 [Fig. 9(d)]. Meanwhile, the smaller S_x and S_y signals in zHanle tests than S_z signal in xHanle tests also prove the stronger out-of-plane magnetic moment at the $\text{Fe}_5\text{GeTe}_2/\text{graphene}$ interface [Fig. 9(f)].

V. GRAPHENE-BASED VERTICAL SPIN VALVE

Although spintronic properties of graphene have been mainly studied for efficient spin transport by lateral spin valve, their integration into the prototypical spintronic devices with vertical spin valve opens another avenue for graphene-based spintronics.^{148,161} Vertical spin valves provide an additional spatial dimension for data storage, further boosting the storage capabilities of hard drives.¹⁶² Moreover, if the vertical spin valves integrate spin-transfer torques or spin-orbit torques, a fast, low-power operation nonvolatile magnetic memory will be achieved.^{163,164} Vertical spin valves are divided into metallic spin valve (MSV) and magnetic tunneling junction (MTJ), which can be distinguished by the intermediate barrier layer in the device structure and by the I-V characteristic curve in electrical transport tests,¹⁶⁵ as shown in Fig. 10. In general, the barrier layer of vertical spin valve is usually ultra-thin, within a few nanometers in thickness.

The most important performance indicator for vertical spin valves is the magnitude of magnetoresistance (MR). The MR in MTJ is also called tunneling magnetoresistance (TMR). Quantitatively, the MR is expressed as $MR = \frac{R_{AP} - R_p}{R_p} \times 100\%$, where R_p and R_{AP} are the resistance of a vertical spin valve when the magnetization of two ferromagnetic electrodes is under parallel and antiparallel states, respectively. A simple model for calculating the spin polarization of two ferromagnetic electrodes was proposed by Jullière in 1975, which is

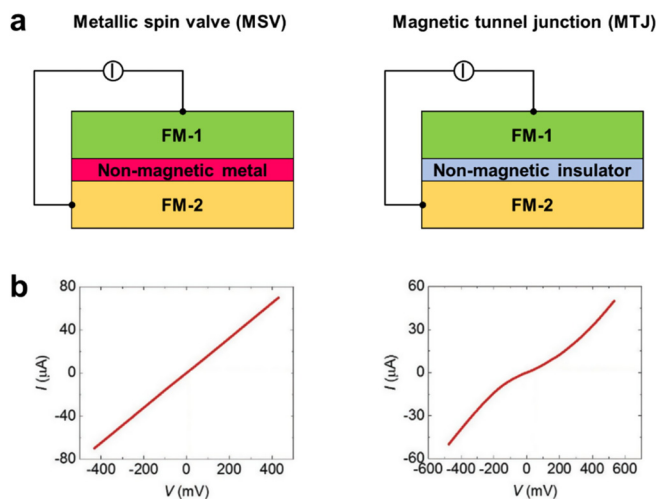


FIG. 10. The difference between metallic spin valve (MSV) and magnetic tunnel junction (MTJ). (a) Device structures of MSV and MTJ. The FM-1 and FM-2 are two ferromagnetic electrodes. (b) Corresponding I-V characteristic curves of MSV and MTJ. Reproduced with permission from Zhu et al., *Adv. Mater.* **33**, 2104658 (2021). Copyright 2021 Wiley-VCH.

expressed as $MR = \frac{2P_1P_2}{1-P_1P_2}$, where P_1 and P_2 are spin polarization of two ferromagnets.¹⁶⁶ Thus, it can be known that the calculated spin polarization depends not only on the intrinsic property of the ferromagnetic electrodes but also on the structures and physical properties of the barrier layer and the heterostructure interface.¹⁶⁷⁻¹⁷⁰ However, in terms of fabricating vertical spin valves, the realization of large MR value by delicately control of structural quality and nanoscale ultra-thin barrier is particularly challenging. For example, if an oxide is used as a barrier in MTJs, growing an ultra-thin pinhole-free barrier that can withstand annealing without breaking the interface, diffusing in the barrier, and oxidizing the ferromagnetic electrodes, remains a key concern. Therefore, in the urgent need to further reduce size and improve performance of spintronic devices, vertical spin valves based on conventional non-van der Waals barriers and interface are often limited by thermal stability, annealing tolerance, and interface quality. 2D materials such as graphene, with their advantages of layer-by-layer thickness control, sharp interfaces, and potential diffusion barrier may provide promising ways to address some of these issues and even achieve some new functionalities such as spin-filtering.^{59,60,168,171}

Till now, graphene-based vertical spin valves have been studied for more than ten years ago.^{148,161} For nearly ten years, the device structures and performances of graphene-based vertical spin valves are summarized in Table III. The studies mainly focus on several device structures, such as Co/Al₂O₃/graphene/Ni,^{59,60,172,173} Co/graphene/NiFe,^{174–176} Ni/graphene/Ni,^{177,178} and NiFe/graphene/NiFe.^{179–181} For example, Grigorieva *et al.*¹⁷⁵ reported the MR of ~1% in Co/

TABLE III. Properties of graphene-based vertical spin valves in the last decade. MR is magnetoresistance, TMR is tunneling magnetoresistance, P is spin polarization, and Gr is graphene.

Structures	MR/TMR (%)	P (%)	T (K)	Year	Ref.
La ₂ Co _{0.77} Mn _{1.23} O ₆ /Gr/MgO/Co	0.48	0.8	2	2023	168
Co/Al ₂ O ₃ /Gr/Ni	-160 82 -6.6 -31	-98 54 -9.8 -42	2 4 1.4 1.4	2022 2020 2015 2014	59 60 172 173
Ni/Gr/NO ₂ -phenyl/Co	-4	...	2	2022	190
Co/Gr/MoSe ₂ /Gr/NiFe	0.33	...	300	2020	184
Co/Gr/NiFe	1.2 1 1.3	8 7 ...	30 10 300	2020 2017 2014	174 175 176
Ni/Gr/Ni	0.1 0.73	...	300	2019	177
Co/Gr/Au/Ni	0.57	6.03	300	2017	178
NiFe/Gr/NiFe	0.29 1.75 4.6	...	300	2016 2015 2014	179 180 181
NiFe/Gr/h-BN/Co	-0.85	...	300	2016	186
NiFe/Gr/Fe	12	24	15	2016	191
NiFe/Al ₂ O ₃ /Gr/Co	-0.53	...	300	2015	187
Co/Gr/Al ₂ O ₃ /Ni	-0.4	...	300	2014	188
La _{2/3} Sr _{1/3} MnO ₃ /Gr/Co	0.63	...	300	2014	189

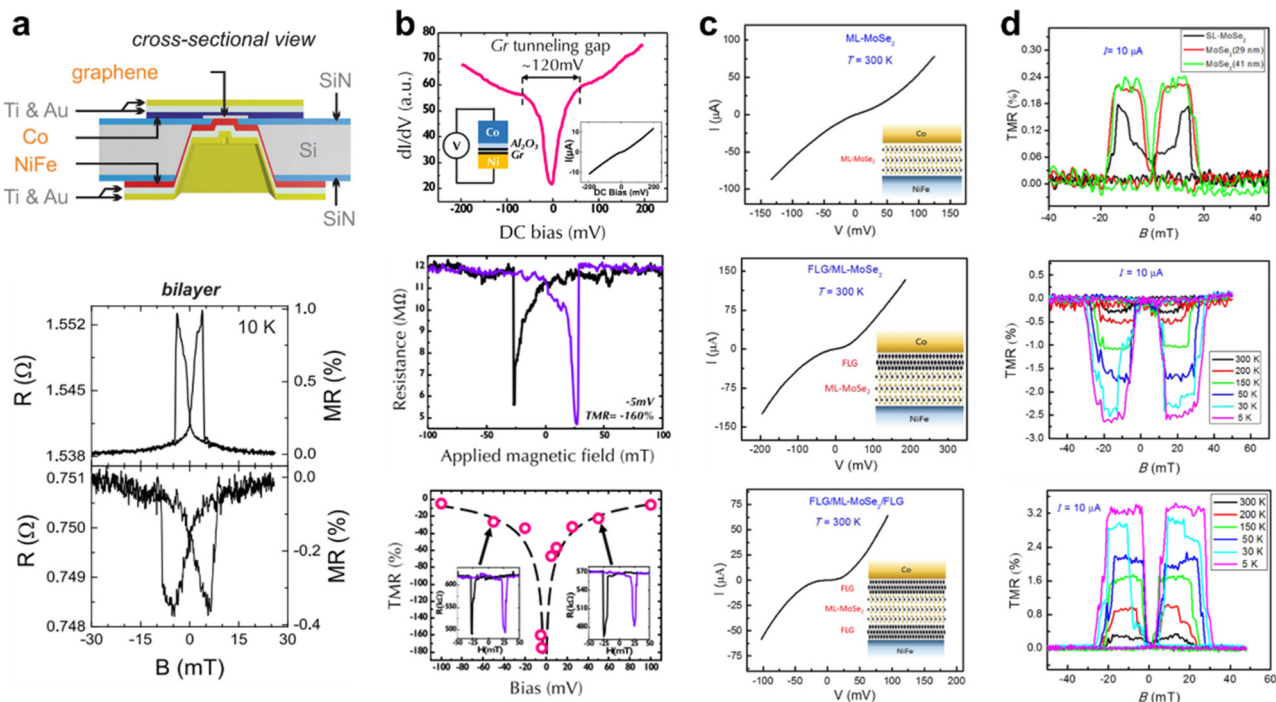


FIG. 11. Graphene-based vertical spin valves. (a) Schematic device structure of Co/graphene/NiFe and corresponding MR curves before and after annealing (300 °C@10 h) at 10 K. Reproduced with permission from Asshoff *et al.*, 2D Mater. **4**, 031004 (2017). Copyright 2017 IOP Publishing. (b) Bias-dependent differential conductance (dI/dV), magnetic field dependent resistance, and bias-dependent TMR of Co/Al₂O₃/graphene/Ni at 2 K. Reproduced with permission from Zatko *et al.*, ACS Nano **16**, 14007 (2022). Copyright 2022 American Chemical Society. (c) and (d) Room-temperature I-V characteristics and corresponding TMR in different device structures. Reproduced with permission from APL Mater. **8**, 071104 (2020). Copyright 2020 AIP Publishing.

graphene/NiFe-based MSV with bilayer graphene at 10 K [Fig. 11(a)]. Moreover, graphene can also be used as a good protective layer to ensure that the ferromagnetic electrodes are not oxidized in the subsequent process of device fabrication. In 2022, Pierre Seneor *et al.*⁵⁹ fabricated the Co/Al₂O₃/graphene/Ni-based MTJ with graphene-protected Ni electrodes. Almost the perfect spin-filtering effect with tunable MR up to −160% and spin polarization ($P_{Ni/graphene}$) up to −98% at 2 K and −5 mV is realized, which is attributed to the highly protected crystallinity and metallic state of Ni(111) ferromagnetic electrode protected by multilayer graphene [Fig. 11(b)]. Such MR and spin polarization are larger than that of other graphene-based vertical spin valves. With the increase in bias, the MR gradually decreases, which is classically ascribed to ferromagnetic magnons.^{182,183} In addition, several studies have demonstrated graphene-based vertical spin valves at room temperature with MR from −0.85% to 1.3%.^{176–179,184–189} Notably, the polarity of TMR is independent of non-magnetic barriers but closely related to the interface between ferromagnets and 2D materials.¹⁸⁴ For example, with the insertion of graphene, the tunneling properties of the Co/MoSe₂/NiFe-based MTJ are gradually obvious at room temperature [Fig. 11(c)]. Meanwhile, the polarity of TMR is changed in Co/graphene/MoSe₂/NiFe-based MTJ, implying the different polarity of spin polarization of Co/graphene and NiFe/MoS₂ interfaces [Fig. 11(d)]. The absence of polarity change of MR in many graphene-based vertical spin valves may be attributed to the unintentional oxidation of the ferromagnetic electrodes during the manufacturing process, making it hard to accurately evaluate the underlying spin-transferring

mechanism.¹⁸⁴ Therefore, the microscopic spin-filtering or spin-transferring effects at the ferromagnet/non-magnet interfaces may be critical for the observed MR anomalies, which need more theoretical and experimental explorations. Moreover, the integrated fabrication and multifunctional devices of room-temperature-operational graphene-based vertical spin valves should be further studied for the practical application of next-generation low-power spintronics.

VI. GRAPHENE-BASED SPIN LOGIC CIRCUITS

The reliable, universal, integrated and reprogrammable spin logic operation with all-electric control is promising for digital electronics and spintronics.^{192,193} Since the realization of long-distance spin communication in large-area multi-terminal graphene spin circuits,^{61–63} graphene has become an ideal candidate for potential spin logic circuits. In 2020, Khokhriakov *et al.*⁶³ demonstrated a complex Y-junction and hexa-arm spin circuit on a wafer-scale graphene film by industry-compatible nanofabrication techniques, as shown in Figs. 12(a) and 12(b). Such a commercially available high-quality graphene film has a long spin transport distance of 34 μm, thereby showing effective communication of spin current between the magnetic memory components in circuit [Fig. 12(c)]. Nevertheless, realizing more complex functions through designing and manufacturing spin logic circuits based on the large-scale graphene film is still lacking.

Recently, the realization of programmable multifunctional spin logic operations in graphene-based spin logic units at room temperature strongly demonstrates the feasibility of graphene for information

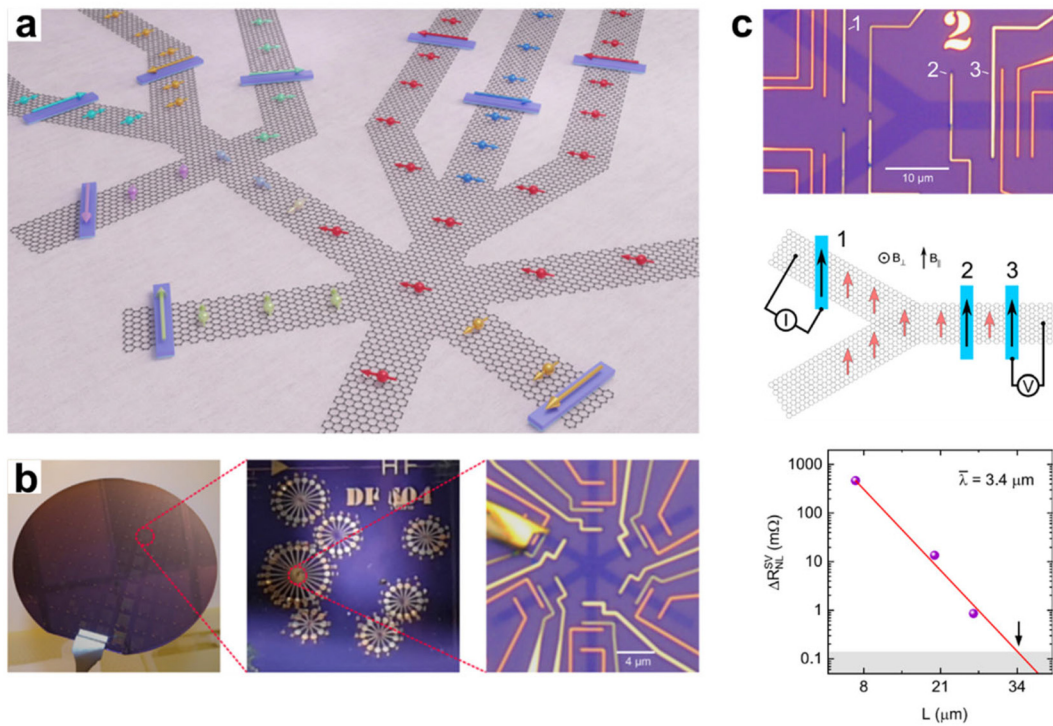


FIG. 12. Graphene-based spintronic circuit architectures. (a) Schematic of a spin circuit formed by interconnecting multiple nano-magnetic components with graphene channels. (b) Images of a spin circuit on a chip from a 4-in. graphene wafer. (c) Optical image, schematic diagram, and channel length-dependent spin valve magnitude of graphene Y-junction spin circuit. Reproduced with permission from Khokhriakov et al., Carbon **161**, 892 (2020). Copyright 2020 Elsevier.

technologies.⁶⁴ Figure 13(a) shows a spin-majority logic device with a three-input fan-in circuit, which consists of the graphene channel, ferromagnetic electrodes (TiO_2/Co), and non-magnetic electrodes (Ti/Au). When two or three inputs input a spin-up current ($+i_S$), the output signal is $+2i_S$ or $+3i_S$, respectively, that is “1” state. When two or three inputs input a spin-down current ($-i_S$), the output signal is $-2i_S$ or $-3i_S$, respectively, that is “0” state [Fig. 13(b)]. In other words, whether 0 or 1 state is related to the spin majority of the input current. Moreover, this graphene spin circuit also shows good spin communication properties, which spin lifetime (τ), spin-diffusion coefficient (D), and spin-diffusion length (λ) are, respectively, calculated as ~ 250 ps, $\sim 0.036 \text{ m}^2 \text{ s}^{-1}$, and $\sim 3 \mu\text{m}$ according to the standard Hanle equation¹² [Fig. 13(c)]. The magnitude of output voltage in Fig. 13(c) is sufficient for the state-of-the-art spin logic operations and is expected to be further improved by reducing the dimension of graphene spin circuits and enhancing the spin polarization of ferromagnetic contacts by utilized hBN,⁵⁷ oxide,¹⁹⁴ or van der Waals magnets.^{97,195} Furthermore, all-electric spin-majority logic operation has been realized in a single graphene-based spin logic unit with three inputs [Fig. 13(d)]. The output voltage signal can be effectively tuned by controlling the input current signal for realizing the different logic states, as shown in Fig. 13(e). Notably, this multifunctional logic operation in a single spin device is expected to reduce the circuit complexity.^{196,197} Such spin-majority logic gate presents a good repeatability without attenuation after several cycles [Fig. 13(f)] and shows promising applications in the future.

This highly improved logic operation in graphene-based spin logic devices is to determine the 0 and 1 states through a current

instead of a magnetic field, which has a great advantage over previously reported XOR spin logic devices in terms of operating speed.¹⁹⁸ In the future, the combination between spin-FETs and spin-majority logic device is expected to realize a complete set of Boolean operations,¹⁹⁹ which should be further investigated. The ultimate goal is to cascade several spin devices with various logic functions for establishing a computational paradigm in which spin is the state variable. It is worth noting that the graphene has been proposed as an all-spin logic-in-memory,²⁰⁰ but its low-power consumption, high-speed operation, and other aspects need to be further explored.

VII. CONCLUSION AND OUTLOOK

Recent experimental studies and advanced device fabrication techniques have demonstrated the advantages of graphene in next-generation spintronics and its promising spin-related physical properties at room temperature, including long spin diffusion length, large spin signal, and relatively long spin lifetime, making it one of the most favorable spin channel materials in spintronics. Despite these, graphene-based spintronics still faces many unknowns and challenges.

First, the manipulation of graphene’s SOC is a foundation for graphene-based spintronics. Although many tuning methods and studies have been proposed, a considerable portion of them is only theoretical studies. Therefore, more experiments are needed to demonstrate the effective and convenient control of graphene’s SOC. Moreover, the delicate control and design of the SOC-related topological band structure in graphene for meeting the practical needs of different spintronic applications are still challenging.

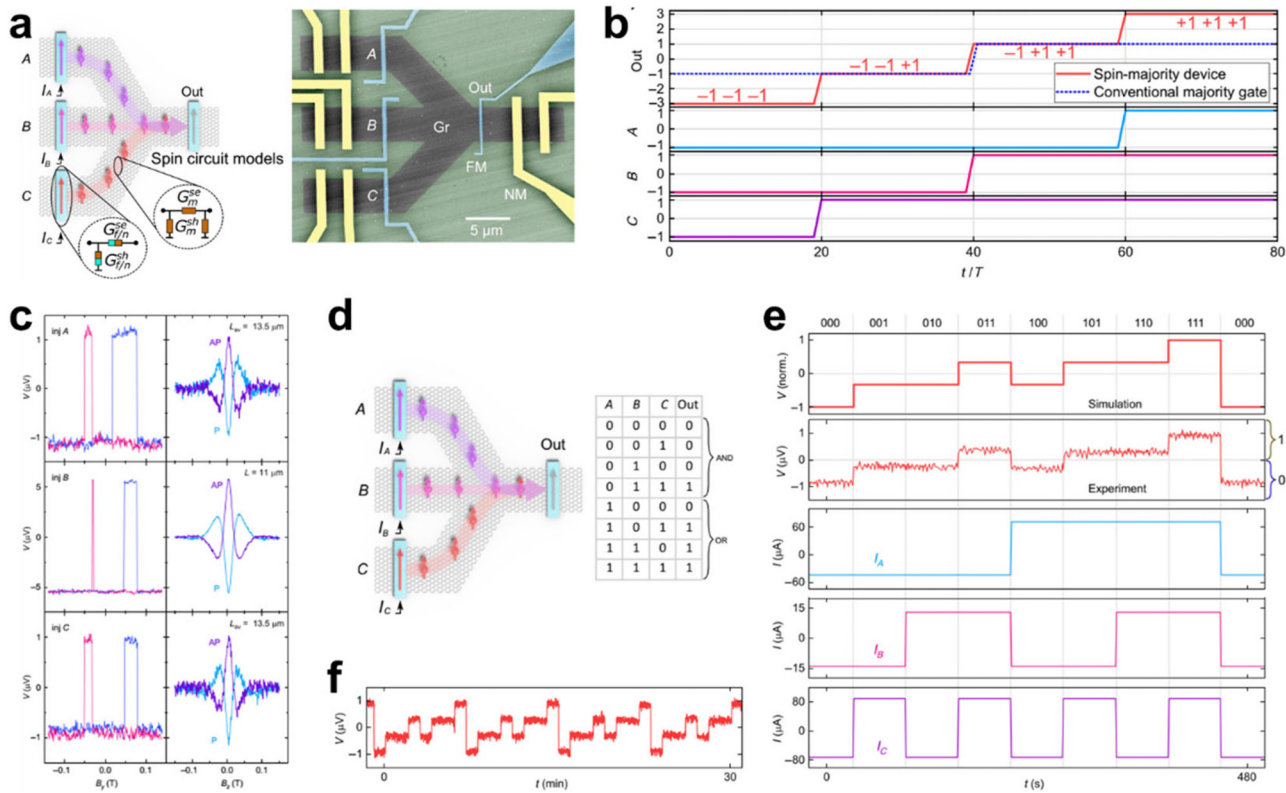


FIG. 13. Room-temperature graphene-based spin logic circuits. (a) Schematic and SEM image of a spin-majority logic device with a three-input fan-in circuit. (b) Simulation comparison of the output signals of conventional majority gate and spin-majority devices under varying input state combinations. (c) Spin-valve and Hanle spin-precession tests of input channels for evaluating the spin communication properties. (d) Schematic of the spin-majority logic device and corresponding truth table for a majority gate. (e) Simulation and experimentally realized logic states probed by applying pulse current to input channels. (f) Performance stability over several cycles. Reproduced with permission from Khokhriakov *et al.*, Phys. Rev. Appl. **18**, 064063 (2022). Copyright 2022 American Physical Society.

24 October 2024 08:42:03

Second, the introduction and regulation of room-temperature long-range magnetic ordered states in graphene are fundamentally important for 2D magnetism and are conducive to promoting the practical application of low-power magnetoelectronic devices. In the past decade, much effort has been made in this field, and some fascinating magnetism-related phenomenon has emerged. However, it is still elusive and very challenging to realize the electrically detectable long-range magnetic order in free-standing graphene. Moreover, the underlying physics of spin-related correlated interactions in magnetic graphene and magic-angle graphene still needs more investigation.

Third, developing large-area graphene-based spintronic devices and achieving highly efficient and reliable spin logic operations will inspire the application of graphene in the next-generation microelectronics industry and quantum technology. However, this poses very strict requirements for the precise design and manufacturing technology of nanodevices, so currently only a few experiments have been done in this regard. Therefore, the fabrication of more novel graphene-based spintronic devices and complex logic circuits for integration with the modern microelectronics industry remain to be explored.

Overall, after witnessing the vigorous development of graphene spintronics over the past ten years, we believe that graphene-based spintronic devices will continue to make more progress in future.

We hope this review will inspire the further development of this attractive and fascinating field.

ACKNOWLEDGMENTS

This work was supported by the National Key Research and Development Program of China (No. 2022YFE0134600), the National Natural Science Foundation of China (Nos. 52272152, 61674063, and 62074061), the Shenzhen Science and Technology Innovation Committee (No. JCYJ20210324142010030), the Natural Science Foundation of Hubei Province, China (No. 2022CFA031), and the Interdisciplinary Research Program of Huazhong University of Science and Technology (No. 5003110122).

AUTHOR DECLARATIONS

Conflict of Interest

The authors have no conflicts to disclose.

Author Contributions

Gaojie Zhang: Conceptualization (equal); Investigation (equal); Methodology (equal); Writing – original draft (equal); Writing – review & editing (equal). **Hao Wu:** Writing – review & editing (equal).

Li Yang: Writing – review & editing (equal). **Wen Jin:** Investigation (equal); Writing – review & editing (equal). **Wenfeng Zhang:** Methodology (equal); Writing – review & editing (equal). **Haixin Chang:** Conceptualization (equal); Methodology (equal); Supervision (lead); Writing – review & editing (equal).

DATA AVAILABILITY

The data that support the findings of this study are available from the corresponding author upon reasonable request.

REFERENCES

- ¹F. Pulizzi, *Nat. Mater.* **11**, 367 (2012).
- ²M. N. Baibich, J. M. Broto, A. Fert, F. Nguyen Van Dau, F. Petroff, P. Etienne, G. Creuzet, A. Friederich, and J. Chazelas, *Phys. Rev. Lett.* **61**, 2472 (1988).
- ³J. S. Moodera, L. R. Kinder, T. M. Wong, and R. Meservey, *Phys. Rev. Lett.* **74**, 3273 (1995).
- ⁴R. E. Camley and J. Barnaś, *Phys. Rev. Lett.* **63**, 664 (1989).
- ⁵S. Lee, J.-H. Chung, X. Liu, J. K. Furdyna, and B. J. Kirby, *Mater. Today* **12**, 14 (2009).
- ⁶P. Barla, V. K. Joshi, and S. Bhat, *J. Comput. Electron.* **20**, 805 (2021).
- ⁷T. Dietl, in *Modern Aspects of Spin Physics*, Lecture Notes in Physics series (Springer, 2007), Vol. 712, pp. 1–46.
- ⁸I. Zutić, J. Fabian, and S. Das Sarma, *Rev. Mod. Phys.* **76**, 323 (2004).
- ⁹F. Schwierz, *Nat. Nanotechnol.* **5**, 487 (2010).
- ¹⁰W. Han, R. K. Kawakami, M. Gmitra, and J. Fabian, *Nat. Nanotechnol.* **9**, 794 (2014).
- ¹¹K. S. Novoselov, A. K. Geim, S. V. Morozov, D. Jiang, Y. Zhang, S. V. Dubonos, I. V. Grigorieva, and A. A. Firsov, *Science* **306**, 666 (2004).
- ¹²N. Tombros, C. Jozsa, M. Popinciuc, H. T. Jonkman, and B. J. van Wees, *Nature* **448**, 571 (2007).
- ¹³W. Han, K. Pi, K. M. McCreary, Y. Li, J. J. Wong, A. G. Swartz, and R. K. Kawakami, *Phys. Rev. Lett.* **105**, 167202 (2010).
- ¹⁴B. Dublak, M.-B. Martin, C. Deranlot, B. Servet, S. Xavier, R. Mattana, M. Sprinkle, C. Berger, W. A. De Heer, F. Petroff, A. Anane, P. Seneor, and A. Fert, *Nat. Phys.* **8**, 557 (2012).
- ¹⁵T. Y. Yang, J. Balakrishnan, F. Volmer, A. Avsar, M. Jaiswal, J. Samm, S. R. Ali, A. Pachoud, M. Zeng, M. Popinciuc, G. Güntherodt, B. Beschoten, and B. Özylmaz, *Phys. Rev. Lett.* **107**, 047206 (2011).
- ¹⁶J. Park, J. Choi, I. Oh, A.-Y. Lee, C. Won Ahn, S. Koo, J.-W. Yoo, and Y. Jo, *Appl. Phys. Lett.* **117**, 203101 (2020).
- ¹⁷A. M. Afzal, M. F. Khan, G. Nazir, G. Dastgeer, S. Aftab, I. Akhtar, Y. Seo, and J. Eom, *Sci. Rep.* **8**, 3412 (2018).
- ¹⁸S. Omar and B. J. van Wees, *Phys. Rev. B* **97**, 045414 (2018).
- ¹⁹Z. Wang, C. Tang, R. Sachs, Y. Barlas, and J. Shi, *Phys. Rev. Lett.* **114**, 016603 (2015).
- ²⁰J. C. Leutnantsmeyer, A. A. Kaverzin, M. Wojtaszek, and B. J. van Wees, *2D Mater.* **4**, 014001 (2016).
- ²¹G. Song, M. Ranjbar, D. R. Daughton, and R. A. Kiehl, *Nano Lett.* **19**, 7112 (2019).
- ²²B. Karpiak, A. W. Cummings, K. Zollner, M. Vila, D. Khokhriakov, A. M. Hoque, A. Dankert, P. Svedlindh, J. Fabian, S. Roche, and S. P. Dash, *2D Mater.* **7**, 015026 (2020).
- ²³C. Tang, Z. Zhang, S. Lai, Q. Tan, and W. B. Gao, *Adv. Mater.* **32**, 1908498 (2020).
- ²⁴D. V. Averyanov, I. S. Sokolov, A. M. Tokmachev, O. E. Parfenov, I. A. Karateev, A. N. Taldenkov, and V. G. Storchak, *ACS Appl. Mater. Interfaces* **10**, 20767 (2018).
- ²⁵B. Zhou, J. Balgley, P. Lampen-Kelley, J. Q. Yan, D. G. Mandrus, and E. A. Henriksen, *Phys. Rev. B* **100**, 165426 (2019).
- ²⁶W. Liu, L. Liu, B. Cheng, H. Qin, G. Zhou, B. Cui, and J. Hu, *Nano Lett.* **22**, 4392 (2022).
- ²⁷H.-D. Song, P.-F. Zhu, J. Fang, Z. Zhou, H. Yang, K. Wang, J. Li, D. Yu, Z. Wei, and Z.-M. Liao, *Phys. Rev. B* **103**, 125304 (2021).
- ²⁸H. Wu, L. Yang, G. Zhang, W. Jin, B. Xiao, W. Zhang, and H. Chang, *Small Methods* **2301524** (published online) (2024).
- ²⁹A. L. Sharpe, E. J. Fox, A. W. Barnard, J. Finney, K. Watanabe, T. Taniguchi, M. A. Kastner, and D. Goldhaber-Gordon, *Science* **365**, 605 (2019).
- ³⁰J.-X. Lin, Y.-H. Zhang, E. Morissette, Z. Wang, S. Liu, D. Rhodes, K. Watanabe, T. Taniguchi, J. Hone, and J. I. A. Li, *Science* **375**, 437 (2022).
- ³¹C.-C. Tseng, X. Ma, Z. Liu, K. Watanabe, T. Taniguchi, J.-H. Chu, and M. Yankowitz, *Nat. Phys.* **18**, 1038 (2022).
- ³²M. He, Y. H. Zhang, Y. Li, Z. Fei, K. Watanabe, T. Taniguchi, X. Xu, and M. Yankowitz, *Nat. Commun.* **12**, 4727 (2021).
- ³³S. Grover, M. Bocarsly, A. Uri, P. Stepanov, G. Di Battista, I. Roy, J. Xiao, A. Y. Meltzer, Y. Myasoedov, K. Pareek, K. Watanabe, T. Taniguchi, B. Yan, A. Stern, E. Berg, D. K. Efetov, and E. Zeldov, *Nat. Phys.* **18**, 885 (2022).
- ³⁴M. Serlin, C. L. Tschirhart, H. Polshyn, Y. Zhang, J. Zhu, K. Watanabe, T. Taniguchi, L. Balents, and A. F. Young, *Science* **367**, 900 (2020).
- ³⁵J. Balakrishnan, G. K. Koon, A. Avsar, Y. Ho, J. H. Lee, M. Jaiswal, S. J. Baek, J. H. Ahn, A. Ferreira, M. A. Cazalilla, A. H. Castro Neto, and B. Ozylmaz, *Nat. Commun.* **5**, 4748 (2014).
- ³⁶H. Yang, M. Ormaza, Z. Chi, E. Dolan, J. Inglá-Ayón, C. K. Safeer, F. Herling, N. Ontoso, M. Gobbi, B. Martín-García, F. Schiller, L. E. Hueso, and F. Casanova, *Nano Lett.* **23**, 4406 (2023).
- ³⁷C. L. Kane and E. J. Mele, *Phys. Rev. Lett.* **95**, 226801 (2005).
- ³⁸Z. Lu, T. Han, Y. Yao, A. P. Reddy, J. Yang, J. Seo, K. Watanabe, T. Taniguchi, L. Fu, and L. Ju, *arXiv:2309.17436* (2023).
- ³⁹T. Han, Z. Lu, Y. Yao, J. Yang, J. Seo, C. Yoon, K. Watanabe, T. Taniguchi, L. Fu, F. Zhang, and L. Ju, *arXiv:2310.17483* (2023).
- ⁴⁰Y. Han, Z. Yan, Z. Li, X. Xu, Z. Zhang, Q. Niu, and Z. Qiao, *Phys. Rev. B* **107**, 205412 (2023).
- ⁴¹F. R. Geisenhof, F. Winterer, A. M. Seiler, J. Lenz, T. Xu, F. Zhang, and R. T. Weitz, *Nature* **598**, 53 (2021).
- ⁴²Y. Cao, V. Fatemi, S. Fang, K. Watanabe, T. Taniguchi, E. Kaxiras, and P. Jarillo-Herrero, *Nature* **556**, 43 (2018).
- ⁴³S. Cao, C. Cao, S. Tian, and J.-H. Chen, *Phys. Rev. B* **104**, 125422 (2021).
- ⁴⁴B. Fülpö, A. Márrfy, S. Zihlmann, M. Gmitra, E. Tóvári, B. Szenthépér, M. Kedves, K. Watanabe, T. Taniguchi, J. Fabian, C. Schönenberger, P. Makk, and S. Csonka, *npj 2D Mater. Appl.* **5**, 82 (2021).
- ⁴⁵B. Yang, E. Molina, J. Kim, D. Barroso, M. Lohmann, Y. Liu, Y. Xu, R. Wu, L. Bartels, K. Watanabe, T. Taniguchi, and J. Shi, *Nano Lett.* **18**, 3580 (2018).
- ⁴⁶S. Irmer, T. Frank, S. Putz, M. Gmitra, D. Kochan, and J. Fabian, *Phys. Rev. B* **91**, 115141 (2015).
- ⁴⁷S. Bhowmik, B. Ghawri, Y. Park, D. Lee, S. Datta, R. Soni, K. Watanabe, T. Taniguchi, A. Ghosh, J. Jung, and U. Chandni, *Nat. Commun.* **14**, 4055 (2023).
- ⁴⁸D. Wang, S. Che, G. Cao, R. Lyu, K. Watanabe, T. Taniguchi, C. N. Lau, and M. Bockrath, *Nano Lett.* **19**, 7028 (2019).
- ⁴⁹T. Naimer and J. Fabian, *Phys. Rev. B* **107**, 195144 (2023).
- ⁵⁰H. González-Herrero, J. M. Gómez-Rodríguez, P. Mallet, M. Moaied, J. J. Palacios, C. Salgado, M. M. Ugeda, J.-Y. Veuillen, F. Yndurain, and I. Brihuega, *Science* **352**, 437 (2016).
- ⁵¹Y. Ge, L. Chen, C. Jiang, J. Ji, Q. Tan, D. Pan, W. Zhang, R. Zhang, E. Janzen, J. H. Edgar, S. Sang, and H. Wang, *Carbon* **203**, 59 (2023).
- ⁵²W. Hu, C. Wang, H. Tan, H. Duan, G. Li, N. Li, Q. Ji, Y. Lu, Y. Wang, Z. Sun, F. Hu, and W. Yan, *Nat. Commun.* **12**, 1854 (2021).
- ⁵³V. K. Paidi, E. Jung, J. Lee, A. T. Lee, M. Shepit, K. Ihm, B. Lee, J. van Lierop, T. Hyeon, and K. Lee, *Adv. Funct. Mater.* **33**, 2210722 (2022).
- ⁵⁴D. Kim, B. Kang, Y.-B. Choi, K. Watanabe, T. Taniguchi, G.-H. Lee, G. Y. Cho, and Y. Kim, *Nano Lett.* **23**, 163 (2022).
- ⁵⁵J. Panda, M. Ramu, O. Karis, T. Sarkar, and M. Venkata Kamalakar, *ACS Nano* **14**, 12771 (2020).
- ⁵⁶M. Drogeler, C. Franzen, F. Volmer, T. Pohlmann, L. Banszerus, M. Wolter, K. Watanabe, T. Taniguchi, C. Stampfer, and B. Beschoten, *Nano Lett.* **16**, 3533 (2016).
- ⁵⁷M. Gurram, S. Omar, and B. J. V. Wees, *Nat. Commun.* **8**, 248 (2017).
- ⁵⁸J. C. Leutnantsmeyer, J. Inglá-Ayón, M. Gurram, and B. J. van Wees, *J. Appl. Phys.* **124**, 194301 (2018).
- ⁵⁹V. Zatko, S. M. Dubois, F. Godel, M. Galbiati, J. Peiro, A. Sander, C. Carretero, A. Vecchiola, S. Collin, K. Bouzehouane, B. Servet, F. Petroff, J. C.

- Charlier, M. B. Martin, B. Dlubak, and P. Seneor, *ACS Nano* **16**, 14007 (2022).
- ⁶⁰M. Piquemal-Banci, R. Galceran, S. M. Dubois, V. Zatko, M. Galbiati, F. Godel, M. B. Martin, R. S. Weatherup, F. Petroff, A. Fert, J. C. Charlier, J. Robertson, S. Hofmann, B. Dlubak, and P. Seneor, *Nat. Commun.* **11**, 5670 (2020).
- ⁶¹A. Avsar, H. Ochoa, F. Guinea, B. Özyilmaz, B. J. van Wees, and I. J. Vera-Marun, *Rev. Mod. Phys.* **92**, 021003 (2020).
- ⁶²J. F. Sierra, J. Fabian, R. K. Kawakami, S. Roche, and S. O. Valenzuela, *Nat. Nanotechnol.* **16**, 856 (2021).
- ⁶³D. Khokhriakov, B. Karpia, A. M. Hoque, and S. P. Dash, *Carbon* **161**, 892 (2020).
- ⁶⁴D. Khokhriakov, S. Sayed, A. M. Hoque, B. Karpia, B. Zhao, S. Datta, and S. P. Dash, *Phys. Rev. Appl.* **18**, 064063 (2022).
- ⁶⁵T. P. Cysne, J. H. Garcia, A. R. Rocha, and T. G. Rappoport, *Phys. Rev. B* **97**, 085413 (2018).
- ⁶⁶Y. Wang, X. Gao, K. Yang, P. Gu, X. Lu, S. Zhang, Y. Gao, N. Ren, B. Dong, Y. Jiang, K. Watanabe, T. Taniguchi, J. Kang, W. Lou, J. Mao, J. Liu, Y. Ye, Z. Han, K. Chang, J. Zhang, and Z. Zhang, *Nat. Nanotechnol.* **17**, 1272 (2022).
- ⁶⁷P. Högl, T. Frank, K. Zollner, D. Kochan, M. Gmitra, and J. Fabian, *Phys. Rev. Lett.* **124**, 136403 (2020).
- ⁶⁸J. O. Island, X. Cui, C. Lewandowski, J. Y. Khoo, E. M. Spanton, H. Zhou, D. Rhodes, J. C. Hone, T. Taniguchi, K. Watanabe, L. S. Levitov, M. P. Zaletel, and A. F. Young, *Nature* **571**, 85 (2019).
- ⁶⁹J.-L. Ge, T.-R. Wu, M. Gao, Z.-B. Bai, L. Cao, X.-F. Wang, Y.-Y. Qin, and F.-Q. Song, *Front. Phys.* **12**, 127210 (2017).
- ⁷⁰A. Kurzmann, Y. Kleeorin, C. Tong, R. Garreis, A. Knothe, M. Eich, C. Mittag, C. Gold, F. K. de Vries, K. Watanabe, T. Taniguchi, V. Fal'ko, Y. Meir, T. Ihn, and K. Ensslin, *Nat. Commun.* **12**, 6004 (2021).
- ⁷¹M. Kurpas, P. E. Faria Junior, M. Gmitra, and J. Fabian, *Phys. Rev. B* **100**, 125422 (2019).
- ⁷²M. Gmitra, S. Konschuh, C. Ertler, C. Ambrosch-Draxl, and J. Fabian, *Phys. Rev. B* **80**, 235431 (2009).
- ⁷³S. Abdellouahed, A. Ernst, J. Henk, I. V. Maznichenko, and I. Mertig, *Phys. Rev. B* **82**, 125424 (2010).
- ⁷⁴J. C. Boettger and S. B. Trickey, *Phys. Rev. B* **75**, 121402(R) (2007).
- ⁷⁵J. Balakrishnan, G. Kok Wai Koon, M. Jaiswal, A. H. Castro Neto, and B. Özyilmaz, *Nat. Phys.* **9**, 284 (2013).
- ⁷⁶A. Avsar, J. Hak Lee, G. K. W. Koon, and B. Özyilmaz, *2D Mater.* **2**, 044009 (2015).
- ⁷⁷M. Gmitra, D. Kochan, and J. Fabian, *Phys. Rev. Lett.* **110**, 246602 (2013).
- ⁷⁸K. Zollner, T. Frank, S. Irmer, M. Gmitra, D. Kochan, and J. Fabian, *Phys. Rev. B* **93**, 045423 (2016).
- ⁷⁹L. Brey, *Phys. Rev. B* **92**, 235444 (2015).
- ⁸⁰D. Marchenko, A. Varykhvalov, M. R. Scholz, G. Bihlmayer, E. I. Rashba, A. Rybkin, A. M. Shikin, and O. Rader, *Nat. Commun.* **3**, 1232 (2012).
- ⁸¹A. Ciattoni, C. Conti, A. V. Zayats, and A. Marini, *Laser Photonics Rev.* **14**, 2000214 (2020).
- ⁸²R. M. Guzman-Arellano, A. D. Hernández-Nieves, C. A. Balseiro, and G. Usaj, *Phys. Rev. B* **91**, 195408 (2015).
- ⁸³M. M. Otkrov, I. I. Klimovskikh, F. Calleja, A. M. Shikin, O. Vilkov, A. G. Rybkin, D. Estyunin, S. Muff, J. H. Dil, A. L. Vázquez de Parga, R. Miranda, H. Ochoa, F. Guinea, J. I. Cerdá, E. V. Chulkov, and A. Arnaud, *2D Mater.* **5**, 035029 (2018).
- ⁸⁴J. Lee and J. Fabian, *Phys. Rev. B* **94**, 195401 (2016).
- ⁸⁵S. Jafarpisheh, A. W. Cummings, K. Watanabe, T. Taniguchi, B. Beschoten, and C. Stampfer, *Phys. Rev. B* **98**, 241402(R) (2018).
- ⁸⁶I. I. Klimovskikh, M. M. Otkrov, V. Y. Voroshnin, D. Sostina, L. Petaccia, G. Di Santo, S. Thakur, E. V. Chulkov, and A. M. Shikin, *ACS Nano* **11**, 368 (2017).
- ⁸⁷B. Yang, M. Lohmann, D. Barroso, I. Liao, Z. Lin, Y. Liu, L. Bartels, K. Watanabe, T. Taniguchi, and J. Shi, *Phys. Rev. B* **96**, 041409(R) (2017).
- ⁸⁸B. Yang, M.-F. Tu, J. Kim, Y. Wu, H. Wang, J. Alicea, R. Wu, M. Bockrath, and J. Shi, *2D Mater.* **3**, 031012 (2016).
- ⁸⁹Y. Li and M. Koslino, *Phys. Rev. B* **99**, 075438 (2019).
- ⁹⁰T. Naimer, K. Zollner, M. Gmitra, and J. Fabian, *Phys. Rev. B* **104**, 195156 (2021).
- ⁹¹E. Rossi and C. Triola, *Ann. Phys.-Berlin.* **532**, 1900344 (2019).
- ⁹²Z. Wang, D. Ki, H. Chen, H. Berger, A. H. MacDonald, and A. F. Morpurgo, *Nat. Commun.* **6**, 8339 (2015).
- ⁹³Z. Khatibi and S. R. Power, *Phys. Rev. B* **106**, 125417 (2022).
- ⁹⁴A. H. Castro Neto and F. Guinea, *Phys. Rev. Lett.* **103**, 026804 (2009).
- ⁹⁵E. McCann and V. I. Fal'ko, *Phys. Rev. Lett.* **108**, 166606 (2012).
- ⁹⁶G. Zhang, H. Wu, L. Zhang, L. Yang, Y. Xie, F. Guo, H. Li, B. Tao, G. Wang, W. Zhang, and H. Chang, *Small* **18**, e2204380 (2022).
- ⁹⁷S. Zhang, H. Wu, L. Yang, G. Zhang, Y. Xie, L. Zhang, W. Zhang, and H. Chang, *Mater. Horiz.* **9**, 559 (2022).
- ⁹⁸W. Jin, G. Zhang, H. Wu, L. Yang, W. Zhang, and H. Chang, *Chin. Phys. Lett.* **40**, 057301 (2023).
- ⁹⁹A. K. Geim and K. S. Novoselov, *Nat. Mater.* **6**, 183 (2007).
- ¹⁰⁰Y. Wang, Y. Huang, Y. Song, X. Zhang, Y. Ma, J. Liang, and Y. Chen, *Nano Lett.* **9**, 220 (2009).
- ¹⁰¹A. K. Singh and B. I. Yakobson, *Nano Lett.* **9**, 1540 (2009).
- ¹⁰²A. Diamantopoulou, S. Glenis, G. Zolnierkiwicz, N. Guskos, and V. Likidimos, *J. Appl. Phys.* **121**, 043906 (2017).
- ¹⁰³Y. Zhang, F. Gao, S. Gao, and L. He, *Sci. Bull.* **65**, 194 (2020).
- ¹⁰⁴O. V. Yazyev and L. Helm, *Phys. Rev. B* **75**, 125408 (2007).
- ¹⁰⁵K. M. McCreary, A. G. Swartz, W. Han, J. Fabian, and R. K. Kawakami, *Phys. Rev. Lett.* **109**, 186604 (2012).
- ¹⁰⁶M. M. Ugeda, I. Brihuega, F. Guinea, and J. M. Gomez-Rodriguez, *Phys. Rev. Lett.* **104**, 096804 (2010).
- ¹⁰⁷R. R. Nair, M. Sepioni, I. L. Tsai, O. Lehtinen, J. Keinonen, A. V. Krasheninnikov, T. Thomson, A. K. Geim, and I. V. Grigorieva, *Nat. Phys.* **8**, 199 (2012).
- ¹⁰⁸H. Zhang, C. Lazo, S. Blugel, S. Heinze, and Y. Mokrousov, *Phys. Rev. Lett.* **108**, 056802 (2012).
- ¹⁰⁹R. R. Nair, I. L. Tsai, M. Sepioni, O. Lehtinen, J. Keinonen, A. V. Krasheninnikov, A. H. Castro Neto, M. I. Katsnelson, A. K. Geim, and I. V. Grigorieva, *Nat. Commun.* **4**, 2010 (2013).
- ¹¹⁰X. Liu, Z. Hao, E. Khalaf, J. Y. Lee, Y. Ronen, H. Yoo, D. Haei Najafabadi, K. Watanabe, T. Taniguchi, A. Vishwanath, and P. Kim, *Nature* **583**, 221 (2020).
- ¹¹¹K. Sawada, F. Ishii, M. Saito, S. Okada, and T. Kawai, *Nano Lett.* **9**, 269 (2009).
- ¹¹²J. Jung and A. H. MacDonald, *Phys. Rev. B* **79**, 235433 (2009).
- ¹¹³Y. W. Son, M. L. Cohen, and S. G. Louie, *Nature* **444**, 347 (2006).
- ¹¹⁴M. Sepioni, R. R. Nair, S. Rablen, J. Narayanan, F. Tuna, R. Winpenny, A. K. Geim, and I. V. Grigorieva, *Phys. Rev. Lett.* **105**, 207205 (2010).
- ¹¹⁵P. Esquinazi, D. Spemann, R. Hohne, A. Setzer, K. H. Han, and T. Butz, *Phys. Rev. Lett.* **91**, 227201 (2003).
- ¹¹⁶J. J. Chen, H. C. Wu, D. P. Yu, and Z. M. Liao, *Nanoscale* **6**, 8814 (2014).
- ¹¹⁷Y. Cao, J. Y. Luo, V. Fatemi, S. Fang, J. D. Sanchez-Yamagishi, K. Watanabe, T. Taniguchi, E. Kaxiras, and P. Jarillo-Herrero, *Phys. Rev. Lett.* **117**, 116804 (2016).
- ¹¹⁸Y. Cao, V. Fatemi, A. Demir, S. Fang, S. L. Tomarken, J. Y. Luo, J. D. Sanchez-Yamagishi, K. Watanabe, T. Taniguchi, E. Kaxiras, R. C. Ashoori, and P. Jarillo-Herrero, *Nature* **556**, 80 (2018).
- ¹¹⁹E. W. Hill, A. K. Geim, K. Novoselov, F. Schedin, and P. Blake, *IEEE Trans. Magn.* **42**, 2694 (2006).
- ¹²⁰M. Popinciuc, C. Józsa, P. J. Zomer, N. Tombros, A. Veligura, H. T. Jonkman, and B. J. van Wees, *Phys. Rev. B* **80**, 214427 (2009).
- ¹²¹P. J. Zomer, M. H. D. Guimaraes, N. Tombros, and B. J. van Wees, *Phys. Rev. B* **86**, 161416(R) (2012).
- ¹²²Y. P. Liu, H. Idzuchi, Y. Fukuma, O. Rousseau, Y. Otani, and W. S. Lew, *Appl. Phys. Lett.* **102**, 033105 (2013).
- ¹²³P. Martin, B. Dlubak, P. Seneor, R. Mattana, M.-B. Martin, P. Lafarge, F. Mallet, M. L. Della Rocca, S. M.-M. Dubois, J.-C. Charlier, and C. Barraud, *Adv. Quantum Technol.* **5**, 2100166 (2022).
- ¹²⁴X. He, C. Zhang, D. Zheng, P. Li, J. Q. Xiao, and X. Zhang, *ACS Appl. Mater. Interfaces* **15**, 9649 (2023).
- ¹²⁵A. Dankert and S. P. Dash, *Nat. Commun.* **8**, 16093 (2017).
- ¹²⁶J. Inglá-Ayres, F. Herling, J. Fabian, L. E. Hueso, and F. Casanova, *Phys. Rev. Lett.* **127**, 047202 (2021).
- ¹²⁷B. Zhao, R. Ngalo, S. Ghosh, S. Ershadrad, R. Gupta, K. Ali, A. M. Hoque, B. Karpia, D. Khokhriakov, C. Polley, B. Thiagarajan, A. Kalaboukhov, P. Svedlindh, B. Sanyal, and S. P. Dash, *Adv. Mater.* **35**, 2209113 (2023).

- ¹²⁸H. Pan, C. Zhang, J. Shi, X. Hu, N. Wang, L. An, R. Duan, P. Deb, Z. Liu, and W. Gao, *ACS Mater. Lett.* **5**, 2226 (2023).
- ¹²⁹G. Zhang, F. Guo, H. Wu, X. Wen, L. Yang, W. Jin, W. Zhang, and H. Chang, *Nat. Commun.* **13**, 5067 (2022).
- ¹³⁰G. Zhang, H. Wu, L. Zhang, S. Zhang, L. Yang, P. Gao, X. Wen, W. Jin, F. Guo, Y. Xie, H. Li, B. Tao, W. Zhang, and H. Chang, *Adv. Sci.* **9**, 2103173 (2022).
- ¹³¹C. Gong, L. Li, Z. Li, H. Ji, A. Stern, Y. Xia, T. Cao, W. Bao, C. Wang, Y. Wang, Z. Q. Qiu, R. J. Cava, S. G. Louie, J. Xia, and X. Zhang, *Nature* **546**, 265 (2017).
- ¹³²B. Huang, G. Clark, E. Navarro-Moratalla, D. R. Klein, R. Cheng, K. L. Seyler, D. Zhong, E. Schmidgall, M. A. McGuire, D. H. Cobden, W. Yao, D. Xiao, P. Jarillo-Herrero, and X. Xu, *Nature* **546**, 270 (2017).
- ¹³³Z. Fei, B. Huang, P. Malinowski, W. Wang, T. Song, J. Sanchez, W. Yao, D. Xiao, X. Zhu, A. F. May, W. Wu, D. H. Cobden, J. H. Chu, and X. Xu, *Nat. Mater.* **17**, 778 (2018).
- ¹³⁴A. M. Afzal, M. F. Khan, and J. Eom, *Electronics* **10**, 2879 (2021).
- ¹³⁵L. Li, J. Zhang, G. Myeong, W. Shin, H. Lim, B. Kim, S. Kim, T. Jin, S. Cavill, B. S. Kim, C. Kim, J. Lischner, A. Ferreira, and S. Cho, *ACS Nano* **14**, 5251 (2020).
- ¹³⁶W. Yan, O. Txoperena, R. Llopis, H. Dery, L. E. Hueso, and F. Casanova, *Nat. Commun.* **7**, 13372 (2016).
- ¹³⁷J. Inglá-Aynés, M. H. D. Guimaraes, R. J. Meijerink, P. J. Zomer, and B. J. van Wees, *Phys. Rev. B* **92**, 201410(R) (2015).
- ¹³⁸M. V. Kamalakar, C. Groenveld, A. Dankert, and S. P. Dash, *Nat. Commun.* **6**, 6766 (2015).
- ¹³⁹Y. K. Luo, J. Xu, T. Zhu, G. Wu, E. J. McCormick, W. Zhan, M. R. Neupane, and R. K. Kawakami, *Nano Lett.* **17**, 3877 (2017).
- ¹⁴⁰Z. M. Gebeyehu, S. Parui, J. F. Sierra, M. Timmermans, M. J. Esplandiu, S. Brems, C. Huyghebaert, K. Garello, M. V. Costache, and S. O. Valenzuela, *2D Mater.* **6**, 034003 (2019).
- ¹⁴¹K. Komatsu, S. Kasai, S.-L. Li, S. Nakaharai, N. Mitoma, M. Yamamoto, and K. Tsukagoshi, *Appl. Phys. Express* **7**, 085101 (2014).
- ¹⁴²I. G. Serrano, J. Panda, F. Denoel, O. Vallin, D. Phuyal, O. Karis, and M. V. Kamalakar, *Nano Lett.* **19**, 666 (2019).
- ¹⁴³A. L. Friedman, O. M. van't Erve, C. H. Li, J. T. Robinson, and B. T. Jonker, *Nat. Commun.* **5**, 3161 (2014).
- ¹⁴⁴J. C. Toscano-Figuerola, N. Natera-Cordero, D. A. Bandurin, C. R. Anderson, V. H. Guarochico-Moreira, I. V. Grigorjeva, and I. J. Vera-Marun, *Phys. Rev. Appl.* **15**, 054018 (2021).
- ¹⁴⁵T. Yamaguchi, Y. Inoue, S. Masubuchi, S. Morikawa, M. Onuki, K. Watanabe, T. Taniguchi, R. Moriya, and T. Machida, *Appl. Phys. Express* **6**, 073001 (2013).
- ¹⁴⁶M. V. Kamalakar, A. Dankert, J. Bergsten, T. Ive, and S. P. Dash, *Sci. Rep.* **4**, 6146 (2014).
- ¹⁴⁷W. Fu, P. Makk, R. Maurand, M. Bräuning, and C. Schönenberger, *J. Appl. Phys.* **116**, 074306 (2014).
- ¹⁴⁸P. Ghising, C. Biswas, and Y. H. Lee, *Adv. Mater.* **35**, 2209137 (2023).
- ¹⁴⁹M. Pudlák, K. N. Pichugin, and R. G. Nazmitdinov, *Phys. Rev. B* **92**, 205432 (2015).
- ¹⁵⁰J. Bušá, M. Pudlák, and R. G. Nazmitdinov, *Phys. Part. Nucl. Lett.* **16**, 729 (2019).
- ¹⁵¹I. M. Vicent, H. Ochoa, and F. Guinea, *Phys. Rev. B* **95**, 195402 (2017).
- ¹⁵²H. Santos, A. Latgé, L. Brey, and L. Chico, *Carbon* **168**, 1–11 (2020).
- ¹⁵³A. W. Cummings, D. L. Duong, V. L. Nguyen, D. Van Tuan, J. Kotakoski, J. E. Barrios Vargas, Y. H. Lee, and S. Roche, *Adv. Mater.* **26**, 5079 (2014).
- ¹⁵⁴A. W. Tsen, L. Brown, M. P. Levendorf, F. Ghahari, P. Y. Huang, R. W. Havener, C. S. Ruiz-Vargas, D. A. Muller, P. Kim, and J. Park, *Science* **336**, 1143 (2012).
- ¹⁵⁵Y. D. Kim, M.-H. Bae, J.-T. Seo, Y. S. Kim, H. Kim, J. H. Lee, J. R. Ahn, S. W. Lee, S.-H. Chun, and Y. D. Park, *ACS Nano* **7**, 5850 (2013).
- ¹⁵⁶M. Gibertini, A. Tomadin, F. Guinea, M. I. Katsonnelson, and M. Polini, *Phys. Rev. B* **85**, 201405(R) (2012).
- ¹⁵⁷J. Martin, N. Akerman, G. Ulbricht, T. Lohmann, J. H. Smet, K. von Klitzing, and A. Yacoby, *Nat. Phys.* **4**, 144 (2007).
- ¹⁵⁸D. Kochan, M. Gmitra, and J. Fabian, *Phys. Rev. Lett.* **112**, 116602 (2014).
- ¹⁵⁹C. R. Dean, A. F. Young, I. Meric, C. Lee, L. Wang, S. Sorgenfrei, K. Watanabe, T. Taniguchi, P. Kim, K. L. Shepard, and J. Hone, *Nat. Nanotechnol.* **5**, 722 (2010).
- ¹⁶⁰A. Avsar, I. J. Vera-Marun, J. Y. Tan, G. K. W. Koon, K. Watanabe, T. Taniguchi, S. Adam, and B. Özyilmaz, *NPG Asia Mater.* **8**, e274 (2016).
- ¹⁶¹M. Piquemal-Banci, R. Galceran, M.-B. Martin, F. Godel, A. Anane, F. Petroff, B. Dlbak, and P. Seneor, *J. Phys. D* **50**, 203002 (2017).
- ¹⁶²C. Chappert, A. Fert, and F. N. Van Dau, *Nat. Mater.* **6**, 813 (2007).
- ¹⁶³H. Kurebayashi, J. H. Garcia, S. Khan, J. Sinova, and S. Roche, *Nat. Rev. Phys.* **4**, 150 (2022).
- ¹⁶⁴H. Yang, S. O. Valenzuela, M. Chshiev, S. Couet, B. Dieny, B. Dlbak, A. Fert, K. Garello, M. Jamet, D. E. Jeong, K. Lee, T. Lee, M. B. Martin, G. S. Kar, P. Seneor, H. J. Shin, and S. Roche, *Nature* **606**, 663 (2022).
- ¹⁶⁵W. Zhu, H. Lin, F. Yan, C. Hu, Z. Wang, L. Zhao, Y. Deng, Z. R. Kudrynskyi, T. Zhou, Z. D. Kovalyuk, Y. Zheng, A. Patane, I. Zutic, S. Li, H. Zheng, and K. Wang, *Adv. Mater.* **33**, 2104658 (2021).
- ¹⁶⁶M. Julliere, *Phys. Lett. A* **54**, 225 (1975).
- ¹⁶⁷J. M. De Teresa, A. Barthélémy, A. Fert, J. P. Contour, F. Montaigne, and P. Seneor, *Science* **286**, 507 (1999).
- ¹⁶⁸V. Zatko, R. Galceran, M. Galbiati, J. Peiro, F. Godel, L. M. Kern, D. Perconte, F. Ibrahim, A. Hallal, M. Chshiev, B. Martinez, C. Frontera, L. Balcells, P. R. Kidambi, J. Robertson, S. Hofmann, S. Collin, F. Petroff, M. B. Martin, B. Dlbak, and P. Seneor, *Nano Lett.* **23**, 34 (2023).
- ¹⁶⁹E. Y. Tsymbal, O. N. Myrasov, and P. R. LeClair, *J. Phys.: Condens. Matter* **15**, R109 (2003).
- ¹⁷⁰W. Zhu, S. Xie, H. Lin, G. Zhang, H. Wu, T. Hu, Z. Wang, X. Zhang, J. Xu, Y. Wang, Y. Zheng, F. Yan, J. Zhang, L. Zhao, A. Patané, J. Zhang, H. Chang, and K. Wang, *Chin. Phys. Lett.* **39**, 128501 (2022).
- ¹⁷¹E. Cobas, A. L. Friedman, O. M. van't Erve, J. T. Robinson, and B. T. Jonker, *Nano Lett.* **12**, 3000 (2012).
- ¹⁷²M. B. Martin, B. Dlbak, R. S. Weatherup, M. Piquemal-Banci, H. Yang, R. Blume, R. Schloegl, S. Collin, F. Petroff, S. Hofmann, J. Robertson, A. Anane, A. Fert, and P. Seneor, *Appl. Phys. Lett.* **107**, 012408 (2015).
- ¹⁷³M.-B. Martin, B. Dlbak, R. S. Weatherup, H. Yang, C. Deranlot, K. Bouzehouane, F. Petroff, A. Anane, S. Hofmann, J. Robertson, A. Fert, and P. Seneor, *ACS Nano* **8**, 7890 (2014).
- ¹⁷⁴P. R. Sharma, P. Gautam, J. Nam, K. S. Kim, and H. Noh, *Mater. Res. Express* **7**, 085603 (2020).
- ¹⁷⁵P. U. Ashoff, J. L. Sambricio, A. P. Rooney, S. Slizovskiy, A. Mishchenko, A. M. Rakowski, E. W. Hill, A. K. Geim, S. J. Haigh, V. I. Fal'ko, I. J. Vera-Marun, and I. V. Grigorjeva, *2D Mater.* **4**, 031004 (2017).
- ¹⁷⁶W. Li, L. Xue, H. D. Abruna, and D. C. Ralph, *Phys. Rev. B* **89**, 184418 (2014).
- ¹⁷⁷Y. Hu, M. Ji, J. Peng, W. Qiu, M. Pan, J. Zhao, Y. Yao, C. Han, J. Hu, L. Pan, W. Tian, D. Chen, Q. Zhang, and P. Li, *J. Magn. Magn. Mater.* **487**, 165317 (2019).
- ¹⁷⁸M. Z. Iqbal, G. Hussain, S. Siddique, and M. W. Iqbal, *J. Magn. Magn. Mater.* **429**, 330 (2017).
- ¹⁷⁹S. Entani, T. Seki, Y. Sakuraba, T. Yamamoto, S. Takahashi, H. Naramoto, K. Takanashi, and S. Sakai, *Appl. Phys. Lett.* **109**, 082406 (2016).
- ¹⁸⁰S. Entani, H. Naramoto, and S. Sakai, *J. Appl. Phys.* **117**, 17A334 (2015).
- ¹⁸¹J.-H. Park and H.-J. Lee, *Phys. Rev. B* **89**, 165417 (2014).
- ¹⁸²S. Zhang, P. M. Levy, A. C. Marley, and S. S. P. Parkin, *Phys. Rev. Lett.* **79**, 3744 (1997).
- ¹⁸³A. M. Bratkovsky, *Appl. Phys. Lett.* **72**, 2334 (1998).
- ¹⁸⁴M. F. Khan, S. Rehman, M. Abdul Rehman, R. U. Rehman Sagar, D-k Kim, H. M. Waseem Khalil, P. A. Shinde, N. ul Hassan, P. R. Sharma, J. Eom, and S. C. Jun, *APL Mater.* **8**, 071104 (2020).
- ¹⁸⁵M. Z. Iqbal, G. Hussain, S. Siddique, and M. W. Iqbal, *J. Magn. Magn. Mater.* **441**, 39 (2017).
- ¹⁸⁶M. Z. Iqbal, S. Siddique, G. Hussain, and M. W. Iqbal, *J. Mater. Chem. C* **4**, 8711 (2016).
- ¹⁸⁷M. Z. Iqbal, M. W. Iqbal, X. Jin, C. Hwang, and J. Eom, *J. Mater. Chem. C* **3**, 298 (2015).
- ¹⁸⁸A. K. Singh and J. Eom, *ACS Appl. Mater. Interfaces* **6**, 2493 (2014).
- ¹⁸⁹F. Li, T. Li, and X. Guo, *ACS Appl. Mater. Interfaces* **6**, 1187 (2014).
- ¹⁹⁰P. Martin, B. Dlbak, R. Mattana, P. Seneor, M. B. Martin, T. Henner, F. Godel, A. Sander, S. Collin, L. Chen, S. Suffit, F. Mallet, P. Lafarge, M. L. Della Rocca, A. Droghetti, and C. Barraud, *Nanoscale* **14**, 12692 (2022).

- ¹⁹¹E. D. Cobas, O. M. van 't Erve, S. F. Cheng, J. C. Culbertson, G. G. Jernigan, K. Bussman, and B. T. Jonker, *ACS Nano* **10**, 10357 (2016).
- ¹⁹²M. Zeng, L. Shen, H. Su, C. Zhang, and Y. Feng, *Appl. Phys. Lett.* **98**, 092110 (2011).
- ¹⁹³C. Feng, J. Xiang, P. Liu, X. Wang, J. Wang, G. Hu, M. Huang, Z. Wang, Z. Zhang, Y. Liu, Y. Lu, and B. Xiang, *Nano Res.* **12**, 2485 (2019).
- ¹⁹⁴S. Singh, J. Katoch, T. Zhu, R. J. Wu, A. S. Ahmed, W. Amamou, D. Wang, K. A. Mkhoyan, and R. K. Kawakami, *Nano Lett.* **17**, 7578 (2017).
- ¹⁹⁵M. Gibertini, M. Koperski, A. F. Morpurgo, and K. S. Novoselov, *Nat. Nanotechnol.* **14**, 408 (2019).
- ¹⁹⁶R. Zhang, K. Walus, W. Wang, and G. A. Jullien, *IEEE Trans. Nanotechnol.* **3**, 443 (2004).
- ¹⁹⁷A. Vayset, O. Zografos, M. Manfrini, D. Mocuta, and I. P. Radu, *AIP Adv.* **8**, 055920 (2018).
- ¹⁹⁸H. Wen, H. Dery, W. Amamou, T. Zhu, Z. Lin, J. Shi, I. Žutić, I. Krivorotov, L. J. Sham, and R. K. Kawakami, *Phys. Rev. Appl.* **5**, 044003 (2016).
- ¹⁹⁹L. Amaru, P.-E. Gaillardon, and G. De Micheli, *IEEE Trans. Comput. Des. Integr. Circuits Syst.* **35**, 806 (2016).
- ²⁰⁰B. Behin-Aein, D. Datta, S. Salahuddin, and S. Datta, *Nat. Nanotechnol.* **5**, 266 (2010).